

Faculty of Medicine
Biomedical Engineering

Master of Science Thesis

Intraoperative 3D ultrasound-based planning for surgical resection of liver tumors

by

Luca Sahli

of Wohlen bei Bern, Switzerland

Supervisors
MSc Iwan Paolucci and Prof. Dr.-Ing. Stefan Weber

Institutions
ARTORG Center for Biomedical Engineering Research, University of Bern

Examiners
Prof. Dr.-Ing. Stefan Weber and MSc Iwan Paolucci

Bern, October 2018

Abstract

Introduction Patients with liver cancer are only curatively treated by surgery. Liver resection surgeries are the gold standard to treat these patients. Image guided navigation approaches are not regularly used in this kind of surgery because the involved registration of preoperative imaging data to the surgical site leads to difficulties with deformations. The aim of this thesis is to conceptualize, implement and evaluate a new approach to navigate in tissue sparing resections without registration. This method would instead intraoperatively reconstruct the liver and create a surgical plan to resect tumors near the liver surface.

Methods Liver reconstruction is done in two steps. First, the surface is reconstructed from a sample of points which were acquired from tracked ultrasound. Only points corresponding to ultrasound images arising from the liver surface are added to the sample. Secondly, the tumor is reconstructed as a sphere. The location and diameter of this sphere are determined from the tracked ultrasound images. After freezing an ultrasound image which shows the largest diameter of the tumor, it is semi-automatically segmented. The center of the segmentation is the tumor center and the diameter is estimated from the segmentation contour. Using the created 3D liver model, a plan to resect the tumor is created by fitting a resection shape which respects the safety margin around it. Finally, to test the resulting approach, two experiments are performed on a liver phantom. The first one was executed to evaluate the accuracy of the reconstructed surface. The second one was an usability test conducted with three surgeons to evaluate the software applicability in the operating room.

Results The accuracy experiment of the reconstructed liver surface shows a median error of 2.57 mm. Most of the accessible liver surface has been reconstructed exactly, but large errors (up to 50 mm) are visible at the edge of the reconstructed surface. The usability test shows that the surgeons find the software useful and that they could imagine to use such a system in the operating room.

Conclusions A method to create an intraoperative model of the liver which can be used to plan resections of tumors near the surface was developed. Experiments to evaluate the method show results that are good in this prototype status and look promising for the future development of this project. It has to be further tested if such an approach is applicable in clinics.

Acknowledgements

Here you may include acknowledgements.

Ich erkläre hiermit, dass ich diese Arbeit selbständig verfasst und keine anderen als die angegebenen Hilfsmittel benutzt habe. Alle Stellen, die wörtlich oder sinngemäss aus Quellen entnommen wurden, habe ich als solche kenntlich gemacht. Mir ist bekannt, dass andernfalls der Senat gemäss dem Gesetz über die Universität zum Entzug des auf Grund dieser Arbeit verliehenen Titels berechtigt ist.

Bern, October 31th 2018

Luca Sahli

Contents

Contents	vii
1 Introduction	1
1.1 The Liver	1
1.1.1 Liver Anatomy	1
1.1.2 Liver Cancer	2
1.2 Liver Resections	3
1.3 Intraoperative ultrasound	4
1.4 Navigation for liver resection surgeries	5
1.4.1 Creation of preoperative 3D-models	6
1.4.2 Registration	6
1.4.3 Tracking modalities	7
2 Problem Statement	9
3 State of the art	11
3.1 Ultrasound based registration of the liver	11
3.1.1 Vessel based	11
3.1.2 Using the surface and vessels combined	12
3.2 Surface registration	12
3.3 Creating models from intraoperative imaging for liver resection surgeries	12
3.3.1 Liver surface - Based on laser range scanner	13
3.3.2 Liver surface - Based on stereo endoscopic images	13
3.3.3 Liver surface and vessels - Based on ultrasound	14
3.4 Deficits of existing solutions	15
3.5 Objectives	15
4 Concept	17
4.1 Overview	17
4.2 Functionalities	18
4.2.1 Surface Reconstruction	19
4.2.2 Tumor Segmentation	21
4.2.3 Resection Planning	22
4.3 Workflow	22
5 Implementation	23
5.1 Surface Reconstruction	24
5.1.1 Surface contact detection	26
5.1.2 Outlier removal	26

5.1.3	Reconstruction Parameters	28
5.2	Tumor Segmentation	29
5.2.1	Initialization method	31
5.2.2	Graph cuts	31
5.3	Resection Planning	32
5.3.1	Cone fitting around resection margin	33
5.4	Visualization for navigation	34
5.4.1	Ultrasound overlay	34
5.4.2	3D model	36
5.5	UI Concept	36
6	Experiments	39
6.1	Surface reconstruction accuracy on a technical phantom	39
6.1.1	Methodology	39
6.1.2	Results	40
6.1.3	Discussion	42
6.2	Usability Test	42
6.2.1	Methodology	42
6.2.2	Results	43
6.2.3	Discussion	43
7	Discussion and Conclusions	45
8	Outlook	47
Bibliography		49
A	Vector and Tensor Mathematics	57
A.1	Introduction	57
A.2	Variable Types	57
B	Another Appendix	59
B.1	Section 1	59
B.2	Section 2	59

Chapter 1

Introduction

The liver is an important organ in the human body that is often affected by cancer. Untreated liver cancer leads to death and the only curative treatment of it is surgery. Liver resection surgery is the gold standard treatment and intraoperative ultrasound is the tool used to navigate during these surgeries because it allows to look into the organ which helps to navigate. However, image guidance is not used regularly in this kind of surgery although it has the potential to improve surgical outcome through increased precision, accuracy and reproducibility.

Conventional approaches create a virtual 3D model of the liver from medical image data prior to the surgery. These models can then be used to plan the resection surgery and to navigate during the intervention. Image to patient registration is the task of aligning the virtual 3D model to the patient's anatomy in the operating room. In order to register, part of the patient's liver is reconstructed intraoperatively to know the actual orientation and position of the organ. Because the liver deforms between the preoperative imaging and the surgery, a rigid registration can not superimpose the virtual and real liver perfectly. To compensate for such deformations is a difficult and unsolved problem today.

Conventional approaches already reconstruct parts of the liver but they use them for registration instead of navigation. This project focuses on the conceptualization, implementation and evaluation of a concept for the creation of an intraoperative 3D model of the liver and the intraoperative resection planning on such a model. Like this, the problems of registration and deformation compensation would not need to be solved any more.

1.1 The Liver

1.1.1 Liver Anatomy

The human liver overlies the gallbladder, is located in the right upper quadrant of the abdomen and has different functions. It produces biochemicals necessary for digestion, synthesizes proteins and detoxifies various metabolites. A human liver weighs normally around 1.5 kg, is the heaviest internal organ and the largest gland of the human body. Two large blood vessels are connected to the liver: the portal vein and the hepatic vein. Both of them subdivide into small capillaries called *liver sinusoids* and then lead to the functional units of the liver known as *lobules*. To refer to the different parts of the liver, it is subdivided into eight segments (Figure 1.1). Each segment has its own vascular inflow and outflow.

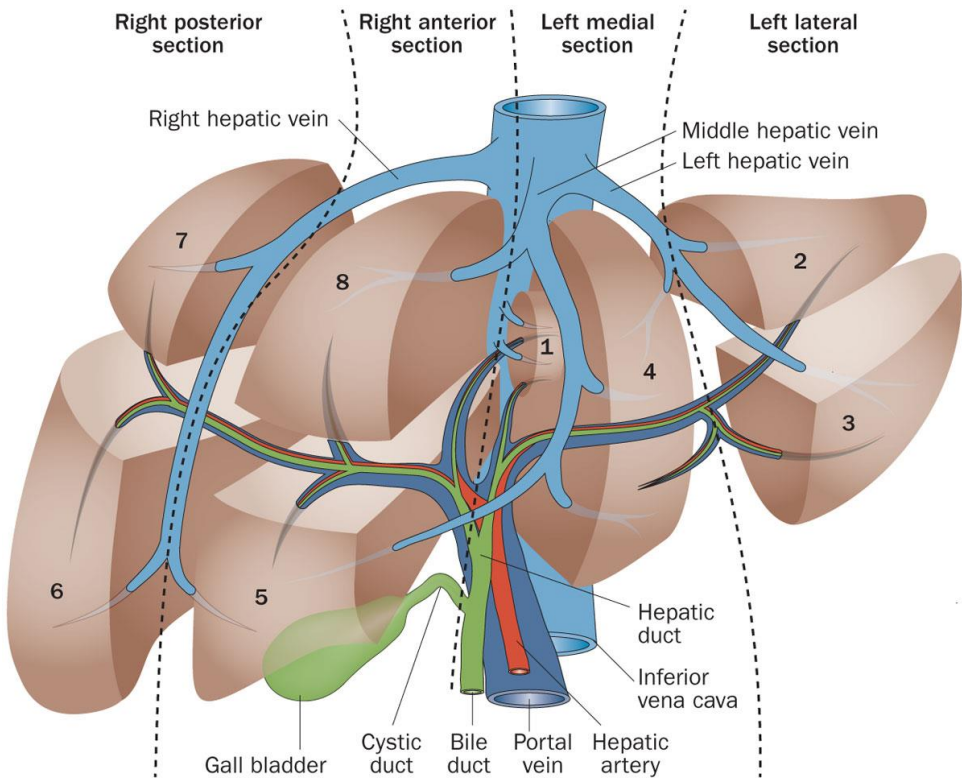


Figure 1.1. The liver and its eight Chouinaud segments. In red is the hepatic artery which transports blood a into the liver. In dark blue the portal vein, it transports blood from the gut into the liver. All the blood leaves the liver through the hepatic veins to the vena cava [62].

1.1.2 Liver Cancer

Liver cancer is cancer that starts in the liver. If the cancer has spread from elsewhere to the liver, then it is known as liver metastasis. Liver metastasis are about 20 times more common in the United States and in Europe than primary tumors. One of the reasons for that is the rich blood supply of the liver which helps the tumors to grow [45]. In Asia it's the other way round, more people suffer from liver cancer than from liver metastases. Liver cancer patients often have chronic liver diseases such as cirrhosis, problems of alcohol abuse, and viral hepatitis (B or C) [30]. The gold standard to treat liver cancer are surgical resections [39]. The liver tissue can easily regrow, given that after resection there is enough healthy tissue and blood supply preserved. Alternatively to resections one can treat liver tumors by local ablation. Both variants treat the tumors with a safety margin of 10 mm. This safety margin ensures that all tumor cells are destroyed and to prevent further spread of cancer cells [43].

1.2 Liver Resections

Hepatectomy is the surgical resection (removal of all or part) of the liver. Liver resections are considered major surgeries and are done under general anesthesia. If no other internal organs of the body are affected and the liver is not cirrhotic, then 70% to 80% of the total liver volume can be removed in a surgical resection. For patients with cirrhotic livers, not more than 50% of the total liver volume should be removed [53]. Liver tissue is cut using instruments like the BiClamp® vessel-sealing device (Figure 1.2). Such devices can simultaneously transect liver parenchyma and seal vessels with diameters smaller than 7 mm [70]. For larger vessels, resorbable clamps are used to prevent heavy bleeding. Most hepatectomies are done laparoscopically. However for complicated cases also open surgeries are done [19].

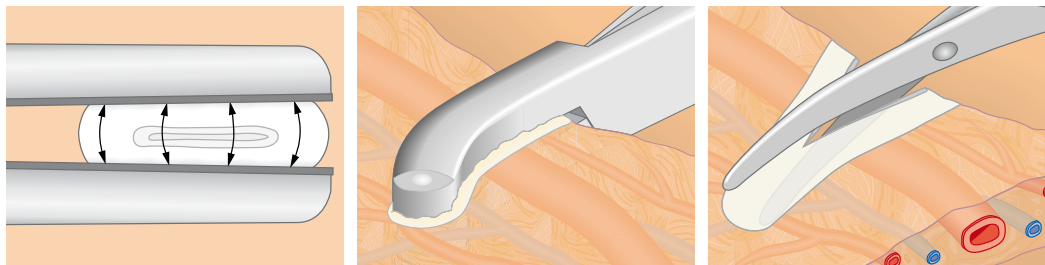


Figure 1.2. A vessel sealing device is used to transect liver parenchyma and split blood vessels then seal them so that no blood is lost. From left to right: First, the vessel is pressed together and then the tissue coagulated using a bipolar electrosurgical current. In some cases this is done twice. Finally the tissue is separated mechanically at the center of the visible coagulation area [1].

Two resection techniques can be separated. Anatomical or parenchymal-sparing resections (Figure 1.3). Most studies analyzing long-term oncological outcomes have shown that there is no significant benefit of anatomical resections over parenchymal-sparing ones in terms of 5-year overall survival and disease-free survival. In anatomical resections (Figure 1.3 A1) the tumors are removed by cutting along anatomical vessel landmarks whereas in parenchymal-sparing resections (Figure 1.3 A2) only the tumor and surrounding tissue is removed such that the safety margin is respected. Parenchymal-sparing resections are shown to be associated with less surgical stress, less postoperative complications and higher feasibility of future resections. This work will concentrate on the parenchymal-sparing technique.

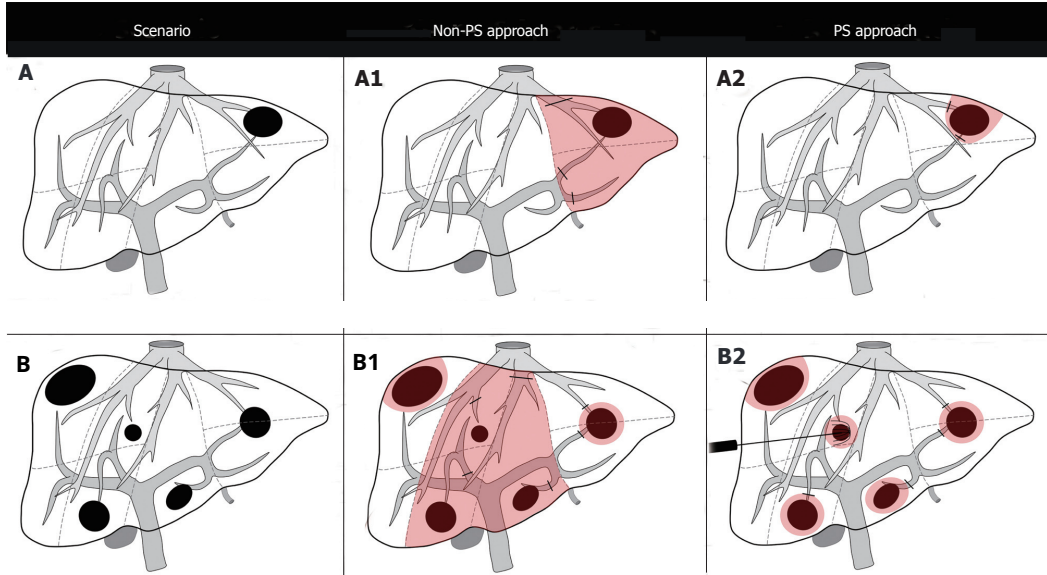


Figure 1.3. Two different approaches to resect liver tumors in two different situations. The *Scenario* column shows the situation of the patient's liver, the *Non-PS approach* column shows how an anatomical resection plan would look like and the *PS approach* column shows how a parenchymal-sparing resection plan would look like [7].

Parenchymal-sparing liver surgeries

Resection is the established gold-standard treatment for liver tumors in general. The surgical treatment of liver tumors has changed with the expansion of the parenchymal-sparing liver resection technique. This technique involves preserving healthy functional liver parenchyma by performing a wide range of liver resections. In order to perform the appropriate type of resection, the site and relationships of the tumor with glissonian pedicles or hepatic veins have to be known. For that reason, it is obvious that only the heavy use of intraoperative ultrasound makes it possible to perform parenchymal-sparing liver resections. Parenchymal-sparing resections are preferably done laparoscopic. This method is backed by technical, oncological, and pathological arguments. This approach has multiple benefits: decreases postoperative mortality and morbidity rates, while preserving the function of the liver. In turn, the risk of liver dysfunction is reduced and the possibility of re-resection in case of recurrence increases. Overall, laparoscopic parenchymal-sparing liver surgeries offer similar survival results compared to open ones [27].

1.3 Intraoperative ultrasound

In liver surgeries an intraoperative ultrasound device is used for intraoperative planning and guidance inside the liver. It is used to locate tumors that are not visible on the liver

surface and to estimate their sizes from the ultrasound image. Figure 1.4 shows an example of an ultrasound image of the liver and its corresponding position in the 3D liver model.

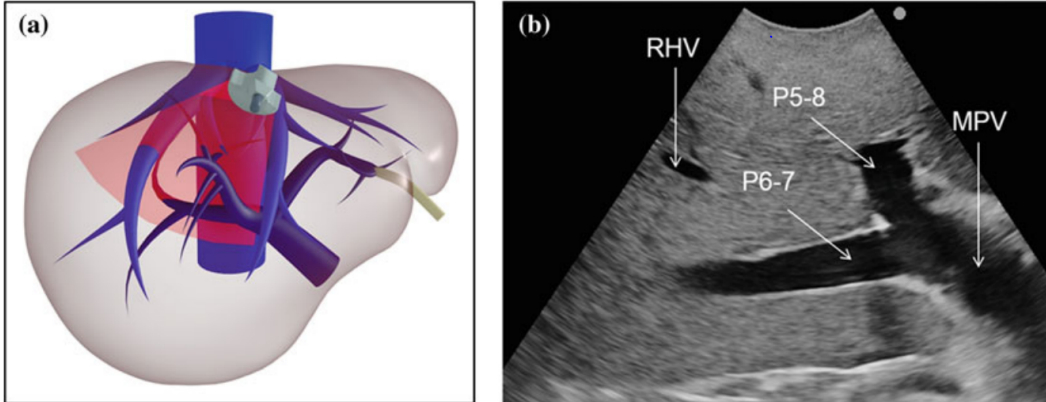


Figure 1.4. Left (a) ultrasound image plane in the liver. Right (b) intraoperative ultrasound image. One can see the right hepatic vein (RHV), the portal branch to segments 5 and 8 (P5-8) and the portal branch to segments 6 and 7 (P6-7) [65]

Ultrasound imaging works by the *pulse-echo* principle. A short ultrasound pulse is emitted from a transducer. The sound waves get transmitted and reflected differently by different tissues. The reflected waves travel back into the transducer and are converted into an electrical signal. After post-processing these signals become ultrasound images. The ultrasound measures the mechanical properties of the tissue. The tissues have different acoustic impedance, which is the product of tissue density and ultrasound speed in travelling through the tissue. The resolution of the ultrasound images depends on the frequency of the ultrasonic waves. High frequencies lead to higher resolution but lower penetration depth into the tissue because the absorption of the sound energy increases with frequency too. Therefore the useability to see deep structures is limited [65].

In liver surgeries ultrasound is an important and established instrument. Intraoperatively, the ultrasound is used on the liver surface directly, therefore the penetration depth of the ultrasound is optimal to represent the inner structures of the liver. Registration methods based on 3D ultrasound reconstructed liver vessels exist but are not used in practice frequently [36]. Ultrasound is not harmful to health and therefore, can be used as often as desired to navigate during a surgery.

1.4 Navigation for liver resection surgeries

It is a difficult task for inexperienced surgeons to orientate themselves within the liver during an operation. From the outside of the liver it is not visible where the blood vessels are which they do not want to hurt. Navigation can help surgeons to orient themselves precisely in organs during operations.

A navigated operation differs in a few points from a non-navigated operation. Because every patient's liver is different, a new 3D model of the liver has to be created before surgery. This models are created from pre-operative 3D computer tomography (CT) scan of the liver. Then, using this model, a surgical plan is made. In contrast to a conventional operation, a navigation system is located in the operating theatre and the surgical instruments can be

tracked by it. Therefore special instruments are used. These instruments have the ability to be tracked by the navigation system. Depending on the tracking technology used by the navigation system, the tools are different. In order to also track the liver, the created model is registered to the anatomy of the patient. Finally the orientation and position of the instruments in relation to the patient's anatomy is visualized on a monitor in the operating room. The surgeon can see what he does on the monitor and uses the system to navigate the location and position of its instruments. This is especially then useful when the tip of the instrument is not actually visible for the surgeon. While the tool tip is not visible, the surgeon has to trust the navigation system. The accuracy of a recently developed system was $4.5 \text{ mm} \pm 3.6 \text{ mm}$ averaged over nine surgeries [52]. Current research tries to compensate for deformations of the liver between the CT scan to the actual shape of the liver during the surgery [21] [22].

1.4.1 Creation of preoperative 3D-models

Several steps are necessary to create a preoperative model. First the CT scan is done. This leads to representations of the liver on several 2D images parallel to each other, filling a square volume with voxels. From this data the liver and its inner structures are manually segmented and merged to a 3D model (Figure 1.5). This is very time consuming and therefore expensive [48]. Nevertheless the resulting models are very detailed and accurate.

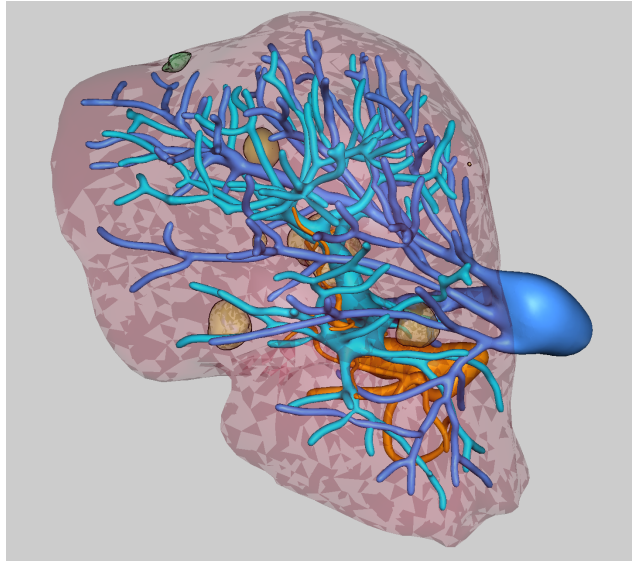


Figure 1.5. Example of a preoperative 3D model created by MeVis

1.4.2 Registration

Patient registration is a concept to correlate the reference coordinate system of a virtual 3D data set with that of a patient. First, the 3D data set has to be gathered. This is often done by CT or MRI scan of the patient's anatomy to be operated on. Secondly, finding of the transformation between the patient's reference coordinate system and the virtual data set. During the surgery the patient is similarly tracked as the instruments (see section 1.4). In this way, the patient has his own coordinate system. From here many different methods

exist to align the virtual data to the real anatomy. Discrete landmarks, surface scans and volumetric sonography scans are just a few of the approaches that can be used to achieve precise alignment of the data with the surgical site [10]. Ultrasound based registration methods in liver surgeries are further discussed in section 3.1.

1.4.3 Tracking modalities

To track surgical instruments and patient's anatomy (define the position and orientation in real time) during naviagated surgery a tracking system is needed. Tracking can be done by different technologies. The most used two tracking modalities are optical and electromagnetic tracking.

1.4.3.1 Optical tracking

Optical tracking is the most used tracking modality in naviagated liver surgeries. Passive markers (spherical, retro-reflective that reflect infrared light) or active markers (infrared-emitting markers that are activated by an electrical signal) [67] are attached to the objects that need to be tracked. A tracking camera is then emitting infrared light by illuminators on the position sensor (only for passive markers). The position sensor determines the position and orientation of the tracked instruments based on the information it receives from those markers [2].

1.4.3.2 Electromagnetic tracking

Electromagnetic (EM) tracking is a modality which uses small coils as markers integrated in surgical instruments. A plate below the patient is used to generate an electromagnetic field which defines the workspace of the tracking system. The position and orientation of the tools in this workspace can be estimated by measuring the signals received by the small coils. This tracking technology does not rely on a line-of-sight and is therefore used in cases where the tracked instruments are inside the patients body.

Chapter 2

Problem Statement

start with the clinical problem that you want to solve why do we need navigation then, and why do we need yet another method? Liver cancer is the fifth deadliest cancer in the world [15]. Primary hepatocellular carcinoma (HCC) and metastatic colorectal hepatic metastasis (CHRM) are the most common hepatic tumours encountered [47]. Worldwide there are 600'000 liver cancer deaths and 700'000 new cases each year. The 5-year survival rate is very low, smaller than 20% for these patients. In Switzerland, around 700 people are diagnosed every year with primary liver cancer. Still, more frequent than primary liver tumours are secondary ones; those that spread as metastases from other organs such as stomach, colon, lungs and breast.

The only way to curatively treat patients with liver tumors is by surgery. Three types of surgery are performed regularly on patients:

- Anatomical resections
- Parenchymal-sparing (non-anatomical) resections
- Tumor ablations

The goal of these treatments is the destruction or removal of the tumor. If the tumor is not visible from the outside of the liver, then it is difficult for the surgeons to tell where exactly it is. Therefore computer assisted navigation could help to locate and visualize it intraoperatively. In the case of liver resection surgeries, navigation systems are rarely employed since they do not provide enough benefits to justify the additional time needed to set them up [12]. These two problems have several origins. First, there is an accuracy problem for registration based approaches. The registration error and the deformations of the liver during the surgery [21] or between the preoperative scan and the surgery lead to errors. Secondly, the time needed to register the patient's anatomy to the preoperative 3D-model. These methods need sometimes multiple attempts to complete a sufficiently accurate registration. Moreover preoperative 3D-models are time consuming and therefore expensive to generate and finally they are deformed anyway such that they better match the actual shape.

In conclusion we aim to develop a new navigation concept based on intraoperative imaging to make computer assisted navigation in liver resection surgeries more accessible to liver surgeons.

Chapter 3

State of the art

This section presents the state of the art in navigation techniques for liver surgery with a focus on approaches tackling the problems of registration during liver surgeries and the challenges when creating 3D models of the liver intraoperatively. Advantages and disadvantages of the different approaches are presented and discussed.

3.1 Ultrasound based registration of the liver

3.1.1 Vessel based

The liver vessels build a complex structure and are therefore well suited for registration. Rigid as well as nonrigid registrations have been studied based on liver vessels [57][37]. On intraoperative ultrasound images the blood vessel sections are visible as black areas within the liver tissue and can be segmented in real time by the use of fast algorithms [57]. Then the vessels are reconstructed to a 3D US model and an ICP algorithm is used to align the vessel model to the preoperative CT data. This method works on a small subvolume of the liver and performs a local rigid registration. It helped to improve the initial manual alignment in 8/14 datasets and in 2/14 the algorithm did not converge [57].

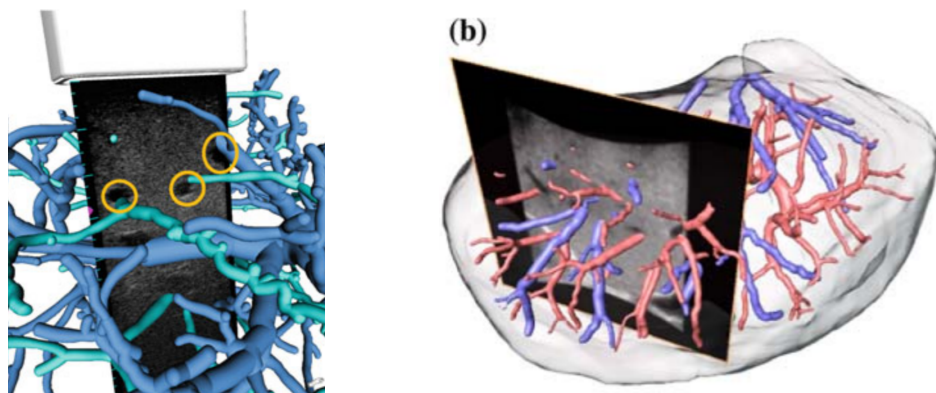


Figure 3.1. Vessel based registration: left [57], right [37]

3.1.2 Using the surface and vessels combined

To combine the inner structure of the vessels with the surface of the liver is an approach to create an automatic registration without the need of an initial alignment. Nam et al. [46] first segment the vessel lumens and the liver surface from 3D B-mode ultrasound images. Then they use an edge matching algorithm to achieve an automatic initial registration based on the vessels. The registration is iteratively refined by jointly using the liver surface and vessel data (Figure 3.2). The achieved average distance between 6-8 anatomical landmarks after automatic registration with this approach was 3.0 mm.

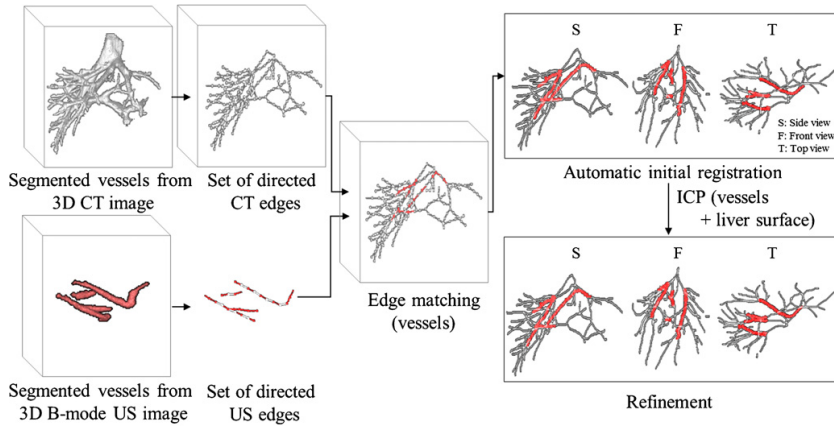


Figure 3.2. Surface and vessel based registration [46]

3.2 Surface registration

Surface registration is registration based on surfaces. It is used and studied for several years in all kinds of fields [55]. Especially in the field of medical technology, a lot of research is being done in the direction of contactless registration. Intraoperatively, different camera technologies which lead to depth images are used to sample the surface of an organ. Often used imaging systems are stereo cameras [29], structured light [60] and laser range scanners [18]. From these intraoperatively created data sets, surfaces are reconstructed and then used for registration. To find the mapping between the surfaces, mostly different variants of the iterative closest point (ICP) [14] algorithm are used.

These surface based methods are limited for different reasons. In most cases only part of the whole organ can be seen (scanned). The scanned surface may lack of unique structures on the surface. The scanning process can lead to noisy data. The organ of interest may be deformed between the acquisitions of the surface samples. Therefore researchers try to compensate for intraoperative soft-tissue deformations [17][25].

3.3 Creating models from intraoperative imaging for liver resection surgeries

In the following subsections intraoperatively created models of parts of the liver are presented. All presented approaches used their reconstructed parts to register the surgical site to the preoperative data.

3.3.1 Liver surface - Based on laser range scanner

Laser range scanners achieve measurements with submillimetric errors and can rapidly acquire thousands of 3D points. In addition to collecting dense surface points, the scanner simultaneously takes images of the visible scene and texture maps the color information onto each surface point (Figure 3.3).

The downside of such an approach is that the laser range scanner takes a lot of space in the operating room and that it only captures the surface data visible from one angle. In addition, only the surface can be reconstructed and no internal structures of the liver.

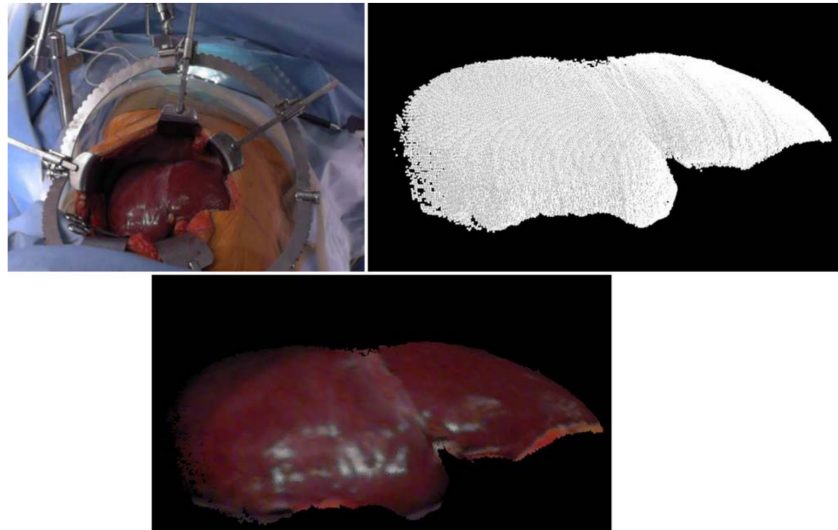


Figure 3.3. Laser range scanning during open surgeries [16]. Top left: This image shows that it is difficult to see a large part of the liver surface from one angle. Top right: The reconstructed surface. Bottom: Reconstructed surface combined with the texture map.

3.3.2 Liver surface - Based on stereo endoscopic images

This approach works for open surgeries as well as for laparoscopic ones. They use a optically tracked stereo endoscope to record the surface of the liver with 20 frames per second intraoperatively and use the images of each frame to create a dense depth image with subpixel precision [63]. From these images the 3D surface positions are calculated. From the growing and resulting point cloud the surface is reconstructed in real time (Figure 3.4).

The disadvantage of this approach is that no internal structures are included in the reconstruction of the intraoperative situation.

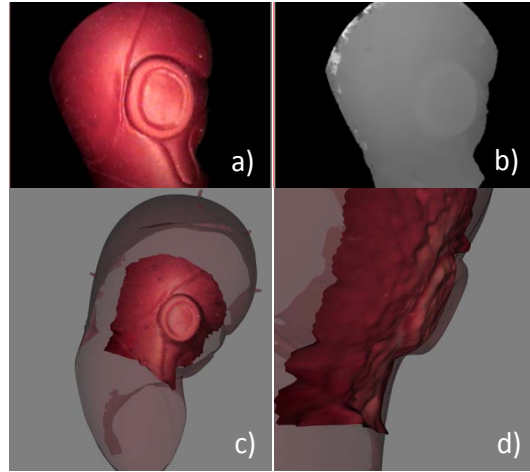


Figure 3.4. Reconstruction of liver phantom. a) The phantom. b) Depth image. c) Initial overlap of the reconstructed point cloud with the tracked liver model. d) Side view [63]

3.3.3 Liver surface and vessels - Based on ultrasound

This approach uses intraoperative ultrasound as the registration tool. It has the advantage that inner and outer structures can be combined. Nam et al. [46] take advantage of the fact that the diaphragm can be made visible on ultrasound images of the liver. At the same time also the vessels are visible on the ultrasound images. Then they automatically segment the large vessels and the part of the liver surface that is attached to the diaphragm. They use the segmentation results to reconstruct the surface and some of the vessels (Figure 3.5). Afterwards they merge the reconstructed vessels and the surface to register to a preoperative model (Figure 3.6).

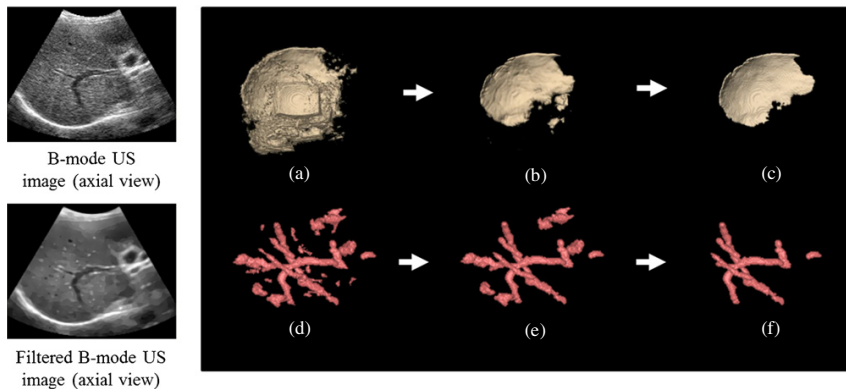


Figure 3.5. Automatic segmentation of the vessels and the surface from filtered 3D ultrasound images and the resulting step by step improved reconstruction [46]

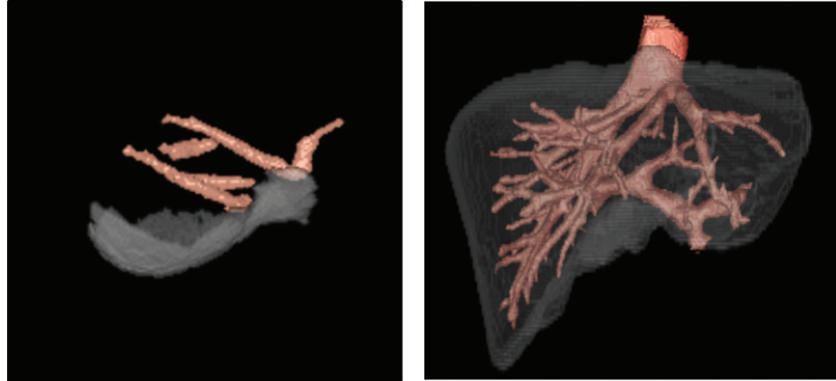


Figure 3.6. Left: The merged reconstruction of the vessels and the surface. Right: The whole liver reconstructed from a CT scan [46]

3.4 Deficits of existing solutions

From the last sections about the state of the art in navigation of liver surgeries a few deficiencies can be spotted. Regarding the ultrasound based registrations, either the reviewed approaches need a time consuming initial semi automatic alignment or have problems with the compensation for deformations of the liver.

Regarding the intraoperative creation of 3D models, some of these approaches lead to incomplete models of the liver anatomy (only the surface). One approach creates a 3D model of the liver surface and vessels using the intraoperative ultrasound. But they use the created 3D model to register to a preoperative CT scan instead of directly navigating using the intraoperatively created 3D model.

To conclude, registration based navigation approaches are error prone and increase intraoperative complexity. So far, no system for liver surgeries allowing intraoperative creation of a 3D model and its use for navigation afterwards exists. Such a system could decrease surgical complexity by eliminating registration from the workflow.

3.5 Objectives

To tackle the challenges described in the previous section, the objectives of this Master's thesis are defined as follows:

- Implementation of a concept for an intraoperative 3D reconstruction technique of the liver from intraoperative ultrasound.
- Implementation of an intraoperative resection planning.

This work focuses on open surgical procedures of parenchymal-sparing liver resections.

Chapter 4

Concept

In this chapter a concept including intraoperative 3D reconstruction of the liver and intraoperative resection planning will be presented.

4.1 Overview

The desired concept differs in some places from conventional approaches, but not everything changes (Figure 4.1). Conventional approaches plan the surgery based on the preoperative CT data very accurately on a 3D model of the liver. Then at the beginning of the surgery, because the liver has probably changed its shape since preoperative scanning, the whole preoperative model (including the preoperative planning) must be deformed again intraoperatively [50].

The new approach is to create a 3D model of the liver during the surgery and plan based on this model. This means that a registration does not have to be done anymore. The created model will not be a complete model of the liver but it will be an undeformed one. Actually, such intraoperative models are already created with conventional approaches, they are only used for registration and not for navigation. Before the planning also the tumor has to be reconstructed intraoperatively.

The hardware for this concept consist of an optical tracking camera, a tracked intraoperative ultrasound and a computer with a 2D and a 3D monitor (Figure 4.2). The tracking camera is used to track the ultrasound and other surgical tools used during the intervention. The ultrasound is used to reconstruct the 3D model of the liver with its tumors and the computer with the monitors is used to visualize the 3D model and planning of the resection. The 2D monitor has a touch interface such that the surgeon can interact with the software.

In order to be able to perform an intervention with this new approach, new functionalities must be developed.

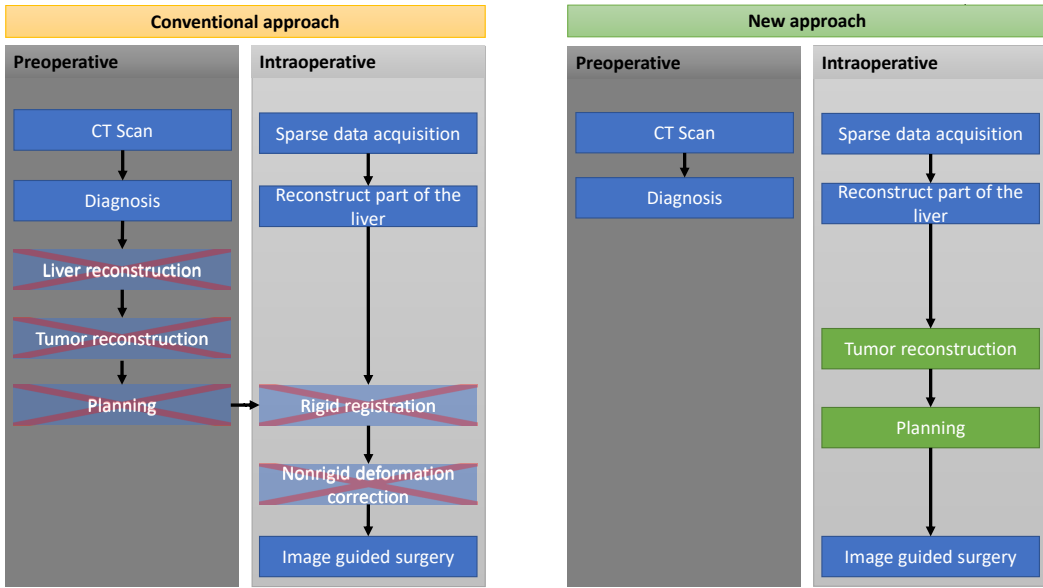


Figure 4.1. The changes from a conventionally navigated liver surgery procedure to the proposed new way of navigating during a liver resection surgery. In the dark gray boxes are the things that are done preoperatively and in the bright gray boxes the things that are done intraoperatively. Boxes with a red cross will not be needed with the new approach and green boxes are not needed with the conventional approach.



Figure 4.2. The setup in the operating room: Red the surgeon; Yellow the tracking camera; Green the ultrasound probe; Dark blue the 3D screen; Light blue the 2D screen.

4.2 Functionalities

The three main functionalities of the developed concept will be presented in this chapter. These functionalities were specifically developed for this project.

4.2.1 Surface Reconstruction

During surgery ultrasound images and their corresponding 6D poses (positions and orientations) are collected and analyzed. First each ultrasound image has to be checked for contact with the liver. If the ultrasound passes the check, that means the ultrasound image looks like an ultrasound image that can only arise when the ultrasound probe lies on the liver surface, then the position of this image can be used.

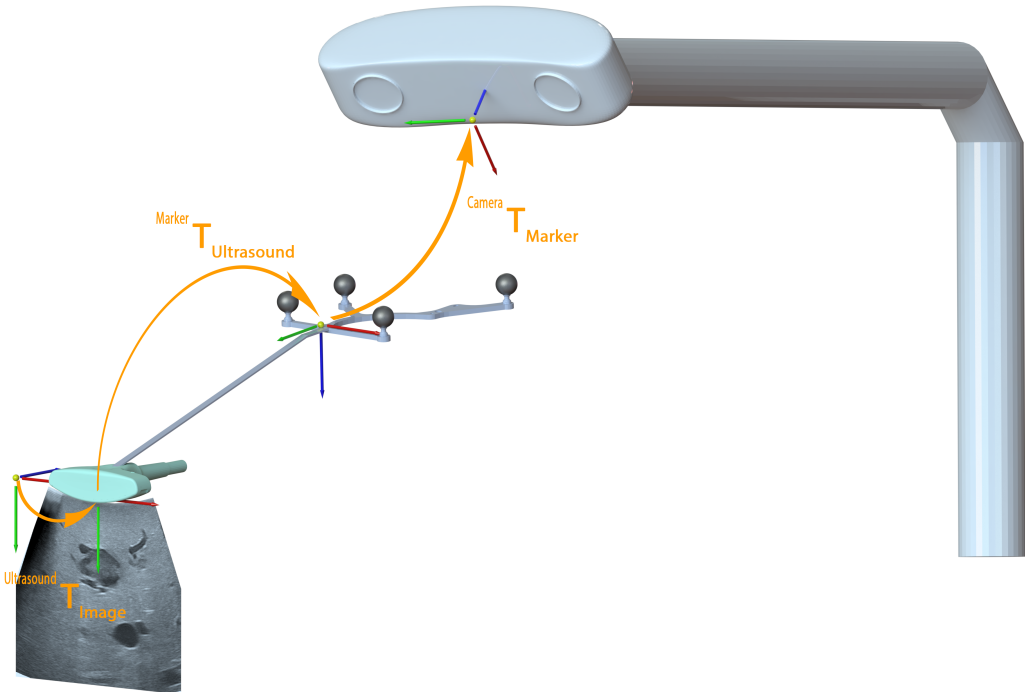


Figure 4.3. The different coordinate systems and the transformations between them.

In order to use ... too complicated. Put an image for that and name the transformations. In order to use the sampled position corresponding to an image, this position has to be transformed into the correct coordinate system first. There are four different coordinate systems (Figure 4.3).

The first coordinate system is the **image coordinate system**. The units in the **image coordinate system** are pixels and the origin is in the top left corner of the ultrasound image. The second coordinate system is the **ultrasound coordinate system**. The origin of this coordinate system is at the probe tip in the middle and the units in this and the other coordinate systems are millimeters. The third coordinate system is the **marker coordinate system**. The origin is at a user defined location, relative to the reflective marker spheres. The final coordinate system is the **camera coordinate system**. The origin of this coordinate system is at the position sensor in the tracking camera and can not be changed.

At the end of this transformation chain, a image pixel 2D position was transformed into a tracking camera 3D positon and the units changed from pixel to millimeter. This 3D

location in the tracking camera coordinate system can be added to the collection of points to later reconstruct the surface from.

After collecting the surface points, a reconstruction algorithm reconstructs the surface from these points.

4.2.1.1 Surface reconstruction from unorganized points

First, collecting the sample ... These terms should match the titles below Both other chapters, explain first what the process is for, then what methods are available A surface reconstruction's goal is to create a surface from sampled points [13]. Two main steps need to be processed. First, acquisition of the data to create a sample. Secondly, apply a reconstruction algorithm on the sampled points.

Data acquisition

what the process is for, then what methods are available In order to reconstruct a surface it is necessary to have some information about it. Therefore a set of points which lie on or near the unknown surface is acquired first. A reconstruction algorithm has then to reconstruct the surface from these points.

There exist different methods to collect surface points [28][40][24][20][26]. Optical (non-contact scan) scans are the most popular ones. Specialy laser based scanners can scan very fast and with a precision in the order of micrometers. Also contact scans exist [49]. Contact scans can also be very precise (in the order of micrometers).

In the field of liver surface scanning only a few articles were published [44] [64]. They used stereo laparoscopic cameras to sample the surface.

Reconstruction algorithms

switch explicit and implicit, so you have the same order as in the figure

what the process is for, then what methods are available The problem surface reconstruction aims to solve is the representation of a surface in digital form, from error containing data that has first been scanned in the real world.

Again, a lot of reconstruction algorithms exist [42], but not all of them are made to reconstruct from unorganized points. This means that the point orders, orientations, connections and the topological type of the surface is not known a priori. Therefore it is necessary that the algorithm does not assume any structure on the data points [33] [69]. The orientations, connections and the topological type must be inferred from the points. This is a major difficulty of the general surface reconstruction problem [32]. In the past few decades, many algorithms that can solve this problem have been published. Nevertheless it is still a challanging task that is part of current research [41]. The available reconstrc-tion types can be classified into two groups: implicit volume-based and explicit mesh-based reconstructions.

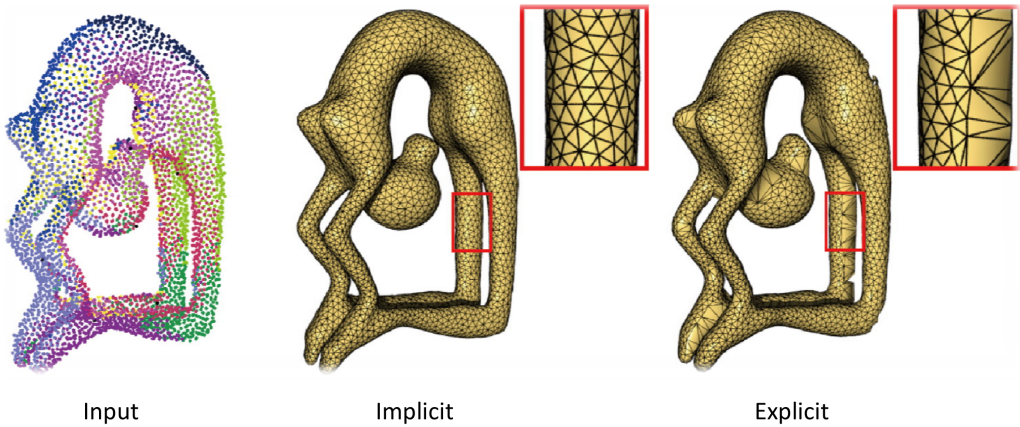


Figure 4.4. The difference between implicit and explicit surface reconstructions. On the left side is the pointcloud used as input. In the middle the result of an implicit reconstruction. On the right side the result of an explicit reconstruction [3]

Implicit volume-based reconstruction

Implicit volume-based reconstruction techniques construct an implicit volume-function from the input points. From the iso-surface of the volume-function a restored surface can then be obtained. For these methods it is not a problem if the surface topology is complex. But most of these methods suffer from oversmoothing the data and the need of accurate directions of normal vectors in addition to the unorganized points.

Explicit mesh-based reconstruction

Explicit mesh-based reconstruction methods form a triangular mesh directly from the unorganized points. These mesh-based reconstructions are precise but they have problems with noise, complex shapes and especially holes in data.

4.2.2 Tumor Segmentation

To reconstruct and later plan the resection of a tumor, the shape of the tumor has to be made visible first. Because most liver tumors are not visible from the outside of the liver, an ultrasound device is often used during liver resections to look behind the liver surface.

Therefore this ultrasound device should also be used to reconstruct the shape of a tumor. This is done by segmenting the same tumor on multiple ultrasound images. Depending on the desired resolution of the reconstructed tumor, more or less images have to be segmented. With the corresponding poses of the ultrasound images, the 3D positions of the individual contour pixels can be calculated. These positions will create a point cloud that represents the shape of the tumor. This shape can then be reconstructed by a surface reconstruction algorithm.

To make an accurate and fast reconstruction of the tumor possible a fast segmentation of the tumor is necessary. For this reason, we employed a semi-automatic segmentation algorithm.

4.2.2.1 Semi automatic 3D segmentation

In order to semi automatically segment a tumor in the liver, the segmentation has to be initialized manually. To do so, a sphere needs to be placed in the center of the tumor manually. Afterwards each ultrasound image which cuts this sphere will be segmented automatically with the cut area as an initialization for the segmentation. These segmentations would be used to reconstruct the surface of the tumor. An accurate reconstruction of the tumor surface would enable for optimized resection planning.

4.2.3 Resection Planning

For parenchymal-sparing liver resections, the goal is to keep as much healthy tissue as possible. When the tumor's location in the liver and the size are known, one can plan a precise resection from these information. The surgeon is able to choose which shape the resection plane will have and how much safety margin he wants to add around the tumor. Then a resection plane which fulfills the desired requirements will be shown to the surgeon. This resection plane could then be fine tuned before the surgeon starts the resection.

4.3 Workflow

In this section the conceptual workflow for a liver resection using the desired system will be presented. The following flow diagram shows the five main steps (Figure 4.5).

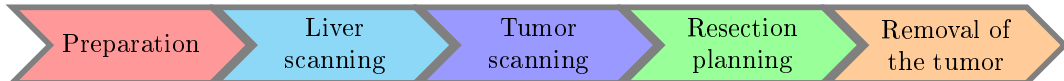


Figure 4.5. The main steps the surgeon has to do during a surgery with the proposed system.

In the preparation step the patient is prepared for the surgery, the navigation system is set up in the operating room and the software is started. Then the tools are setup. Afterwards the surgery starts, the intervention starts and the liver gets prepared for the resection. Subsequently step two starts. In this step the surgeon scans the liver surface with an ultrasound probe. He does that until the liver surface-part needed for the surgery is reconstructed. Thereafter follows the tumor scanning step. Here the surgeon locates a tumor using the ultrasound probe again. Then he freezes the ultrasound image and initializes its segmentation. After this the surgeon moves the ultrasound probe in different directions such that the ultrasound images cut through the tumor. He does that until the tumor is accurately enough reconstructed. Afterwards follows step four. To plan the resection the surgeon has to select the shape of the resection plane he wants to apply for this resection intervention. If necessary he adjusts the resection plane manually. Finally he uses the created model and plan to resect the tumor.

Chapter 5

Implementation

This chapter will explain how the described concept has been implemented. First an overview of the concept and then the main parts of the software are explained in more detail. The trackable marker is attached to the ultrasound probe. The marker is detectable by the tracking camera and enables the camera to determine the position and orientation of the ultrasound probe. The probe on its own will create an ultrasound image. Then the sampled ultrasound image and pose will be post processed as a pair. Depending on the actual state in the surgery, the use of the that pair will be different (Figure 5.1).

The following sections will explain the details of the implemented software parts.

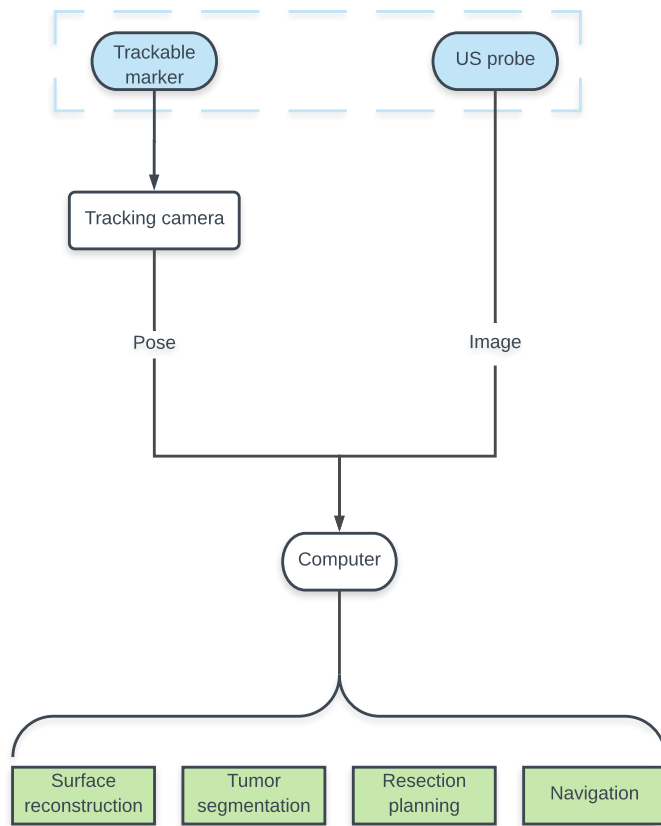


Figure 5.1. This flow chart shows how the ultrasound image and the corresponding pose reach the computer and later to the different parts in the software.

5.1 Surface Reconstruction

While the surgeon is scanning the surface, the software in the background filters out unusable positions. An image pose pair has to pass two tests to become accepted in the group of surface points. The image has to prove that it arised from the liver surface and the position has to have a similar distance to its neighbors as its neighbors to it. When enough points are sampled, the reconstruction of the surface will be carried out.

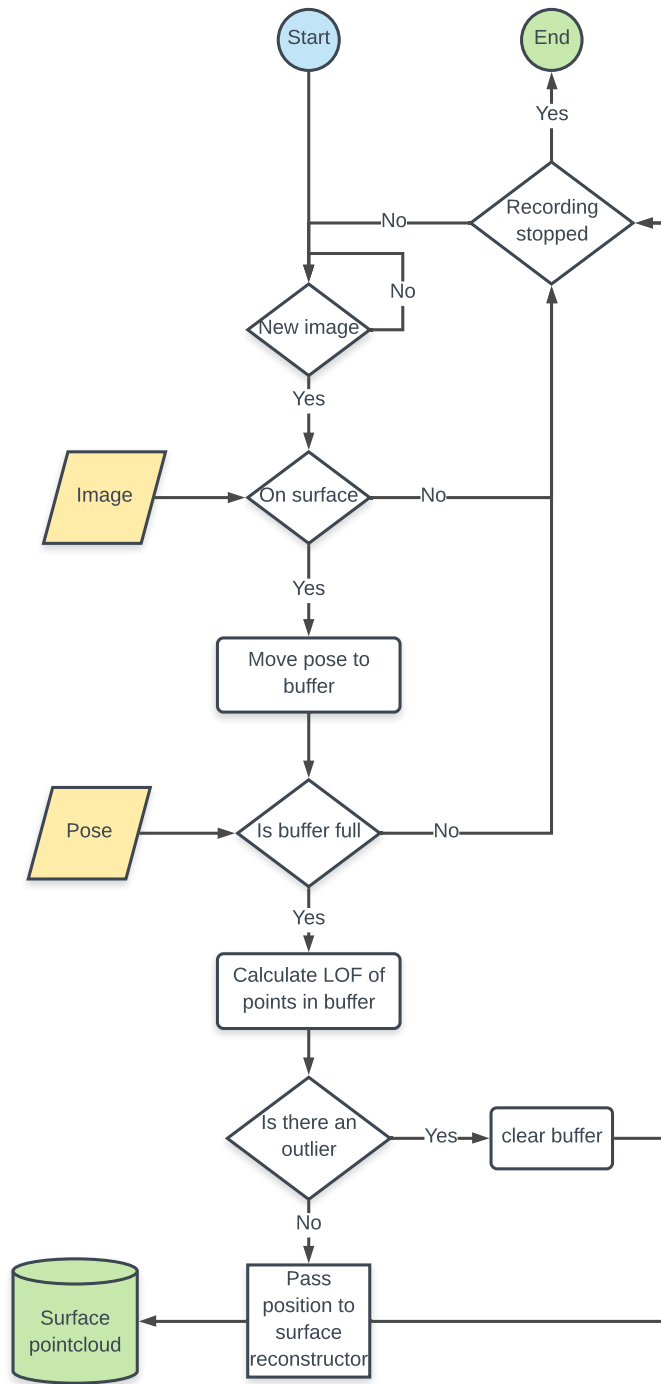


Figure 5.2. This flow chart shows how the image and its pose are checked and used while the surgeon is scanning the liver surface.

5.1.1 Surface contact detection

For an image pose pair, the first step to pass is the contact detection. Only the ultrasound image is needed in this step.



Figure 5.3. Three ultrasound images from left to right: No contact with the liver, difficult to decide (In this case it would be contact because the middle part of the image shows contact), contact with the liver

A classifier detects whether the US probe has contact to the liver or not. Therefore, a support vector machine (SVM) was trained with US images from the phantom and from previous navigated liver surgeries. The SVM was trained to classify the image into “no surface contact” (left) and “surface contact” (middle and right). The images were labelled as “surface contact” if at least 50% and the center had contact to the surface (Figure 6.4 middle). The classifier takes into account that US waves are reflected at the US probe-air interface when the US probe has no contact to the liver and therefore no image is formed. The features for the classifier were: mean, median, minimum, maximum, variance, skewness and kurtosis of the pixel values. All features are calculated on the upper half of the image. For training, a set of 2'311 images (1'056 with contact, 1'255 without contact) were used. The training data was composed of images from a phantom (88%) and images from previous navigated liver surgeries (12%). All computations were performed using the openCV software package.

When the image is classified as “surface contact”, then the position of the pose is stored into the buffer. The buffer has a capacity of 10 positions. When the addition of the actual pose leads to a full buffer, the buffer is tested for outliers. Each time a “no surface contact” image is classified and the positions buffer is not empty it gets cleared.

5.1.2 Outlier removal

To find outliers in the current buffer the local outlier factor is calculated for each position.

The local outlier factor is a numerical value that describes the local density of a position compared to its k-nearest neighbors (Figure 5.4).

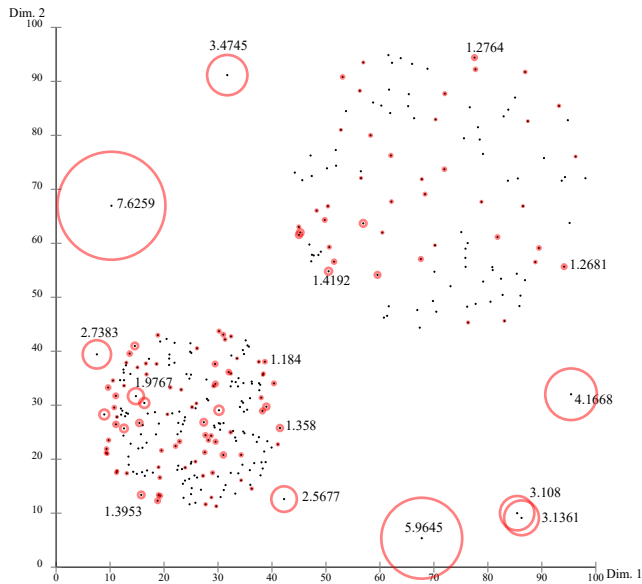


Figure 5.4. Example of the local outlier factors in a two dimensional pointcloud [23].

Five steps can be separated to find the LOF of one position.

1. For each point calculate the distance to all the other points in the buffer
2. For each point find the distance to his k-nearest neighbor → *k-distance*
3. Find the *reachability distance* from the k-nearest neighbors of each point to it self
4. Calculate the *local reachability density* for all points
5. Calculate the *local outlier factor*

The *reachability distance* of point *A* from another point *B* is defined:

$$\text{reachability-d}_k(A, B) = \max\{\text{k_d}(B), d(A, B)\}$$

The *k-distance* of point *B* depends on its k-nearest neighbors and does not need to include point *A*. But the actual distance between point *A* and *B* depends on only *A* and *B*. The larger of the two will be the *reachability distance* of point *A* from point *B*.

The *local reachability density* of a point *A* describes its neighborhood and is defined by:

$$\text{LRD}(A) := 1 / \left(\frac{\sum_{B \in kNN(A)} \text{reachability-d}_k(A, B)}{|kNN(A)|} \right)$$

In words this is the inverse of the sum of the *reachability distances* of point *A* from its k-nearest neighbors devided by *k*.

Finally the *local outlier factor* of a point A indicates how his neighborhood compares with the neighborhoods of his k-nearest neighbors. The LOF of A is defined by:

$$\text{LOF}(A) := \frac{\sum_{B \in kNN(A)} \overline{\text{LRD}}(B)}{|kNN(A)|}$$

If the neighborhood of A is very similar to the neighborhoods of its k-nearest neighbors, the LOF is close to 1. If its neighborhood is less dense than the neighborhoods of his k-nearest neighbors, the LOF becomes larger than 1. If its neighborhood is more dense than the neighborhoods of his k-nearest neighbors, the LOF becomes lower than 1.

If an outlier is found in the buffer, the whole buffer is cleared. In the case that no outlier is found, the oldest pose in the buffer gets moved into the point collection to reconstruct the surface from.

5.1.3 Reconstruction Parameters

Finally there is a pointcloud with all the collected positions. This pointcloud will be used as input for the surface reconstruction algorithm by Hoppe [32]. The algorithm consists of three phases. From an unorganized set of points, phase 1 constructs an initial dense mesh. Starting with the dense mesh created in phase 1, phase 2 reduces the number of faces and improves the fit to the data points. In phase 3, the surface representation is changed from a piecewise linear one (meshes) to a piecewise smooth one. For the computations the implementation in VTK (SurfaceReconstructionFilter) was used. The two main parameters of this reconstruction algorithm have been optimized by applying the grid search method.

5.1.3.1 Grid search for parameter optimization

The *neighborhood size* and the *sample spacing* are the variable parameters of the used surface reconstruction algorithm. The *neighborhood size* specifies the number of neighbors each point has. These neighbors are used to estimate the local surface orientation. The *sample spacing* sets the spacing of a 3D sampling grid. To find the optimal values to use in the algorithm with the point cloud data produced in the experiment described in section 6.1, a first, rough grid search has been done to find the range of interest of the two parameters. The same data was then used to do a second, more dense grid search over the range of interest (Figure 5.5 and 5.6). For each parameter setting, the average distance from the reference points to the reconstructed surface was calculated. The found mean distance varies from 5.1 mm to 3.9 mm. Neighborhood sizes smaller than 8 show an increase of the mean distance for sample spacings larger than 25 mm. Neighborhood sizes over 30 seem to increase the mean distance also. The standard deviation (STD) of the mean varies between 6.1 mm and 4.6 mm. These high deviations result mostly from the boarder part of the reconstructions where the reference points are more than 2 cm away from the surfaces (see section 6.1). One can say the standard deviation of the mean decreases together with the neighborhood size used for the reconstruction. But this is only true for neighborhood sizes larger than 13. Because from neighborhood size 13 till 10 the standard deviation increases not till then it decreases again. By simply summing up the mean and the standard deviation, one finds that the optimal parameters for the tested surface samplings are 13 for the neighborhood size and 30 mm for the sample spacing.

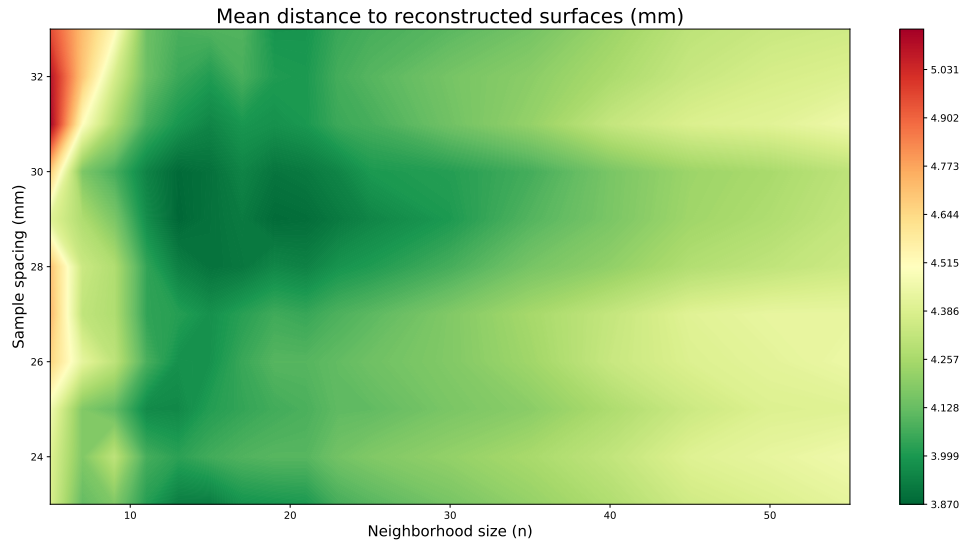


Figure 5.5. This contour plot shows the mean distance calculated over 10 differently sampled point collections. All point collections represent the surface of the same liver phantom.

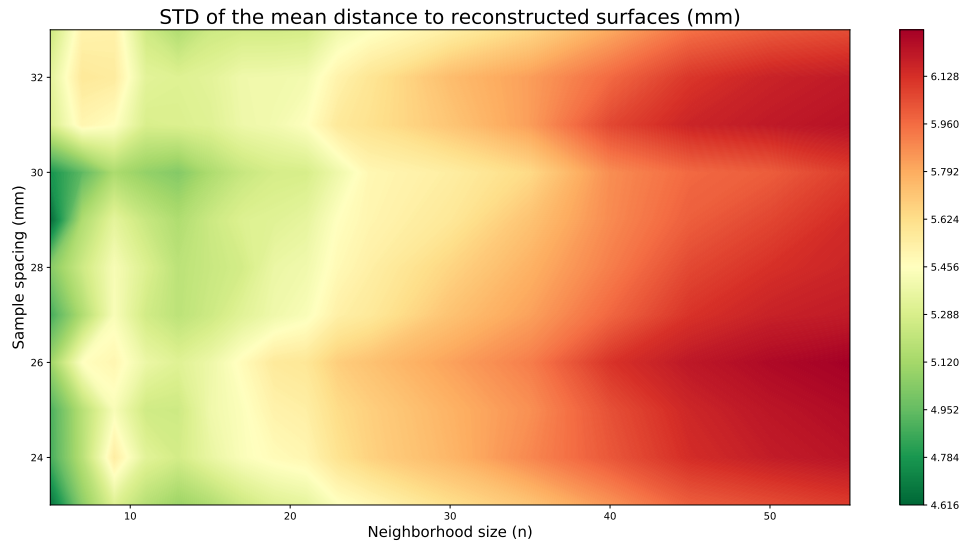


Figure 5.6. This contour plot shows the standard deviation (STD) of the mean distance calculated over 10 differently sampled point collections. All point collections represent the surface of the same liver phantom.

5.2 Tumor Segmentation

The flow diagram in figure 5.7 helps to understand the following explanation of the creation of a tumor 3D model. To create a 3D model of a tumor, the surgeon has to freeze an ultrasound image such that the real tumor center is visible on this image. To find the location of the tumor's center, the surgeon locates the tumor with the ultrasound. Then he freezes the ultrasound image that cuts through the middle of the tumor. The 6D pose of

that ultrasound image is stored and the image is passed to the next step.

Most tumors have roundish shapes, and a sphere is the easiest geometrical shape that can be used to approximate a tumor's real shape. To define a sphere two components are needed: the location and the radius of the sphere.

To get more information about the tumor, the tumor on the freezed image has to be segmented. This segmentation is obtained semi automatically. That means the surgeon has to roughly initialize the segmentation manually and then the graph cut algorithm implemented by OpenCV will segment the the tumor. From the resulting segmentation shape, the tumor center and radius are estimated. The center corresponds to the mean of the segmented boarder pixels and the radius is the mean between the largest and the shortest distance from the boarder pixels to the estimated center pixel. By using the 6D pose corresponding to the ultrasoud image used for the segmentation, the center pixel gets transformed into the tracking camera coordinate system. Finally the sphere that approximates the tumor can be drawn into the same coordinate system as the liver surface.

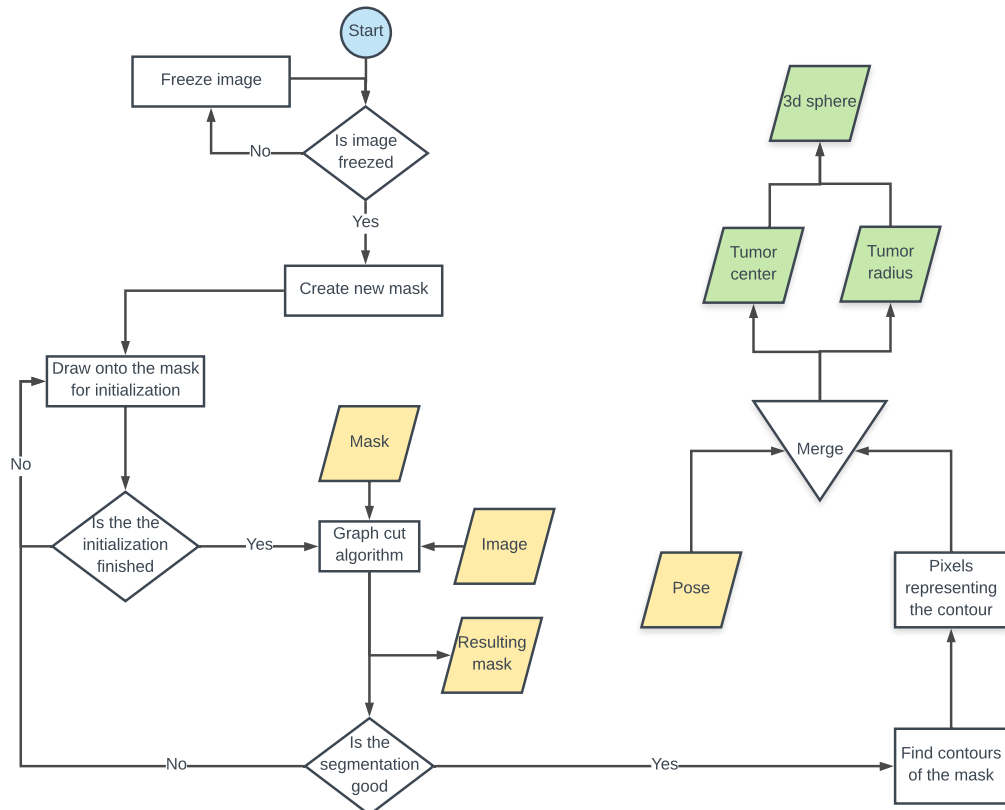


Figure 5.7. This flow chart shows how the image and its pose are used to create a sphere that represents a tumor in the reconstructed liver model.

5.2.1 Initialization method

As explained in section 5.2, the segmentation of the tumor has to be initialized manually. This is done by drawing onto an initialization mask. The surgeon draws two circles onto the mask. After clicking in the middle of the tumor, two circles are drawn onto the mask. An orange circle for the pixels that should be looked at to find the boundary of the tumor (Figure 5.8). And a red circle to color pixels surely originating from the tumor. Most of the time the two circles need to be increased or decreased in size. This is done by clicking the plus or minus buttons. Both circles are changed at the same time. The position can be changed by using the arrow buttons. As soon as the segmentation is satisfactory for the surgeon, he confirms the initialization and the created initialization mask is passed to the segmentation algorithm.

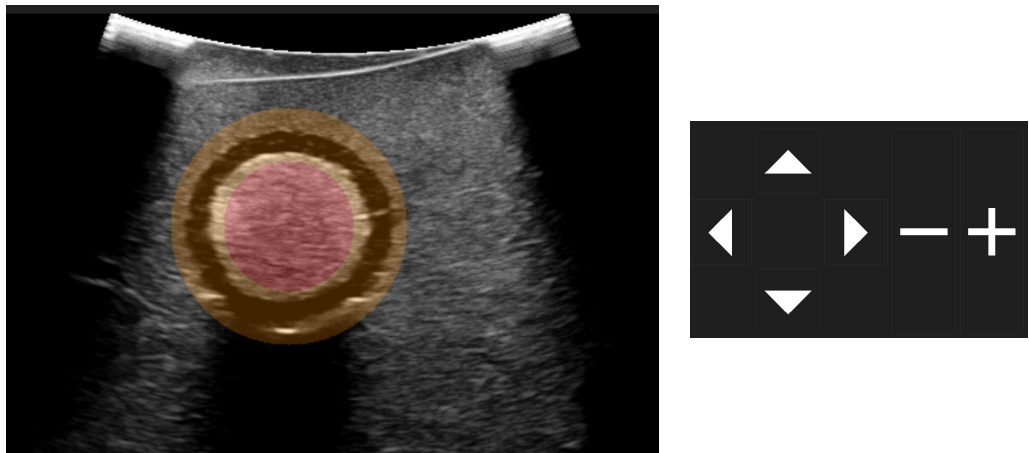


Figure 5.8. On the left side: Initialization drawing for the segmentation of the tumor. Red the pixels which are tumor pixels. And orange the pixels that are from the tumor or the background. The not colored pixels represent background. On the right side: Controls to manipulate the initial segmentation.

5.2.2 Graph cuts

For the segmentation a graph cuts algorithm is used. This algorithm treats pixels as set of nodes connected in a graph (Figure 5.9). Foreground and background are initialized by selecting parts in the image. Pixels labeled foreground belong to the source and background labeled ones to the sink. The nodes (pixels) are connected to their neighbors, the source, and the sink by edges whose weights are defined as follows:

- Node to source → Probability of the node to belong to the source (foreground)
- Node to sink → Probability of the node to belong to the sink (background)
- Node to adjacent node → Similarity measure to its neighboring node.

A weight of an edge to adjacent node depends on the similarity between pixel intensities. The edges between adjacent nodes, initialized to the same label, have an infinitely high weight [66].

After calculating all the weights in the graph, it has to be cutted in order to create a segmentation. All pixels not assigned already in advance foreground or background will get

assigned by cutting the graph. The segmentation is obtained in form of a min-cut [9] in which edges are removed to separate source and sink, and sum of their weights is minimized. This way you can find a group of foreground and background pixels.

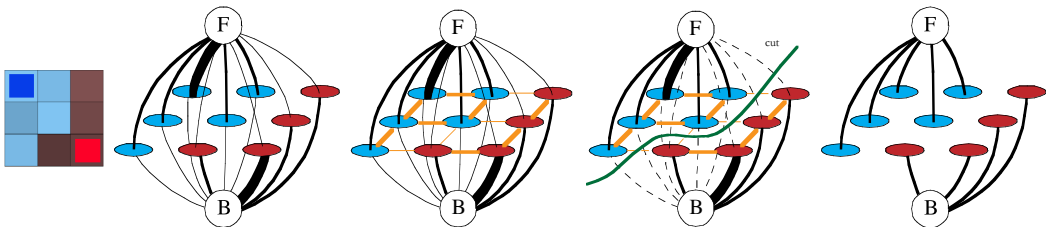


Figure 5.9. From left to right the steps of a graph cut segmentation. The first image shows the nine pixels to separate into foreground and background. A clear blue and a clear red drawing onto two pixels indicate the initialized foreground and background. The second image illustrates the probabilities of each pixel belonging to the foreground or the background. The third image shows the edges between neighboring pixels in orange. The fourth image shows the edges to be cut as dashed lines. Finally the last image shows the result for foreground and background [9].

5.3 Resection Planning

The 3D models of the liver and the tumor are created. In this section we will explain how the resection plane is calculated and displayed in the 3D scene. In order to make better planning possible, the nearest point to the tumor center on the surface of the liver must first be determined. To find this point, the *vtkCellLocator* class is used. This class has a function that can be used to find the nearest point on a surface to a given point and the distance between them. The found point and distance together with the polygonal data of the liver surface, tumor, value for the safety margin, and the desired resection shape are then passed into the resection calculator (Figure 5.10).

The resection calculators task is to create a resection plane under the given conditions and to represent it in the 3D model. It also shows the safety margin taken into account as a sphere around the tumor. In addition, also a help line is displayed on the liver surface to show where the surgeon could start the resection.

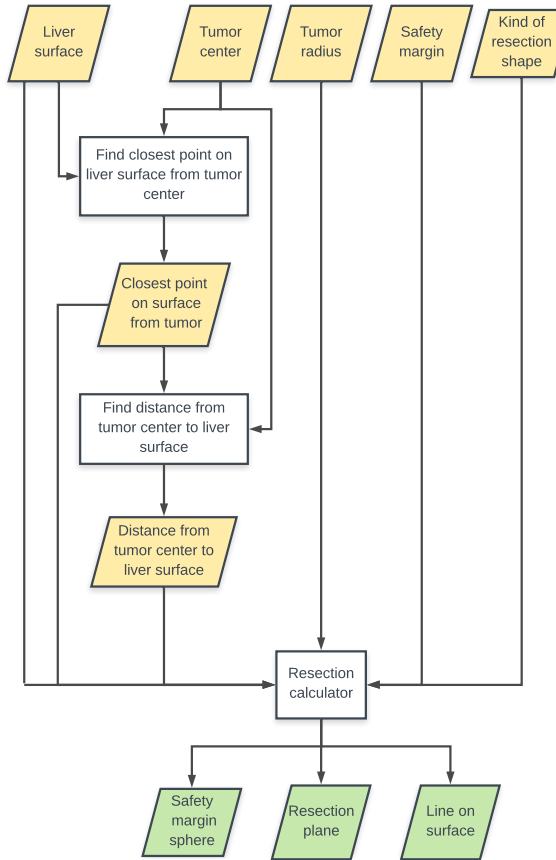


Figure 5.10. This flow chart shows the data flow to and from the resection calculator.

5.3.1 Cone fitting around resection margin

In order to keep as much healthy tissue as possible and still remove the tumor while maintaining the necessary safety margin around the tumor, the resection plane is recalculated for each tumor. Depending on the distance (d) between tumor center (C) and liver surface the angle α varies between 10° and 30° . For tumors with a distance less than 10 mm the angle is fixed to 30° and for distances larger than 30 mm the angle is fixed to 10° . The direction of the cone is defined by the vector from the tumor center to the nearest point (P) on the surface. After constraining the cone to be tangential to the sphere of the safety margin on both sides, the position of the cone apex (A) can be calculated. By enforcing the cutting of the cone tangential to the sphere of the safety margin, the length of the cone is limited towards the apex. The base of the cone is defined to be 10 mm further away from the tumor than the surface point. Finally we have the shape, size and position of the cone that leads to a tissue sparing resection of the given tumor.

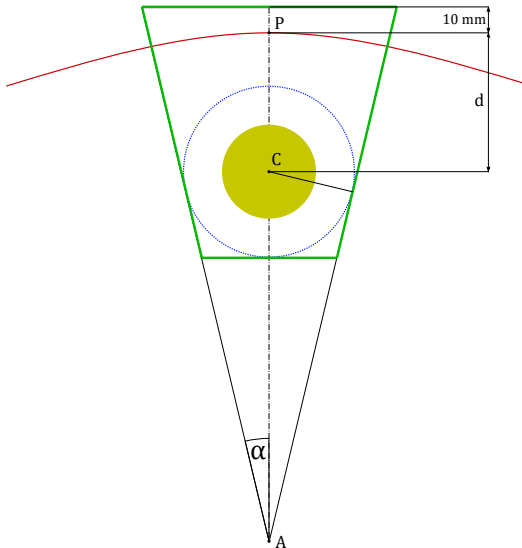


Figure 5.11. The geometrical shape of the resection plane (green) after fitting it around the safety margin (blue). The angle α depends on the distance (d) between the tumor center (C) and the closest point (P) on the liver surface to it. The position of the apex (A) can be calculated after constraining the safety margin to be tangential to the sides of the cone.

5.4 Visualization for navigation

The visualization of the previously created, virtual, assisting, 3D models to the surgeon should make the intervention safer or even improve it. We use a 3D screen to show the 3D scene. This makes it easier for the surgeon to move the surgical tools while looking at the 3D scene. Because surgeons need the ultrasound device a lot during liver resections, it makes sense to combine the 3D models with the ultrasound image.

5.4.1 Ultrasound overlay

By blending the contours of all visible models (except the liver surface) which cut the image plane, with the live ultrasound image, the 3D models become visible on the ultrasound image (Figure 5.13). Figure 5.12 explains how an image and its corresponding pose are used to cut the 3D scene and blend the contours with the live image. First, the pose is used to check if the image cuts an object in the scene. This is done with the *vtkCutter* class. This class can simulate a cut through a 3D object with an implicit function. The implicit function of an image is a plane, and therefore simple to create by using the image pose. Because the cutter can only return a binary mask of where it cuts an object, the cutter has to check each object separately. Each time the returned mask from the cutter is not empty, contour of the mask is found by using the openCV function *findContours*. The found contour is then colored depending on the color of the cutted 3D object and added to the mask which will be finally blended with the original image. If an object is fully transparent (not visible on the 3D screen), then also the countour line will be fully transparent. The described procedure is performed for each new ultrasound image during the navigated intervention.

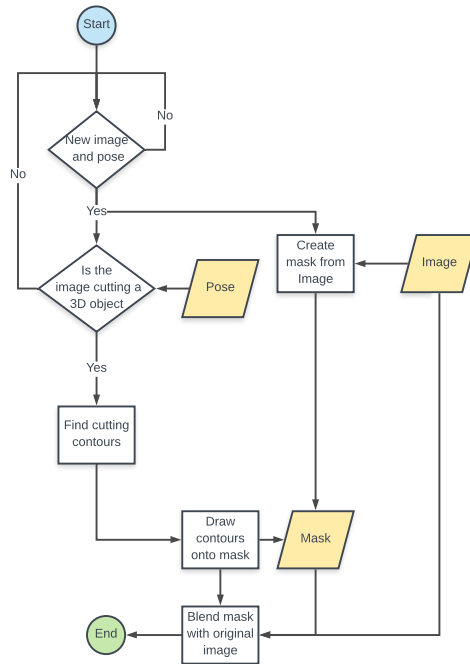


Figure 5.12. This flow chart shows the data flow to create the overlay of the 3D objects onto the live ultrasound images.

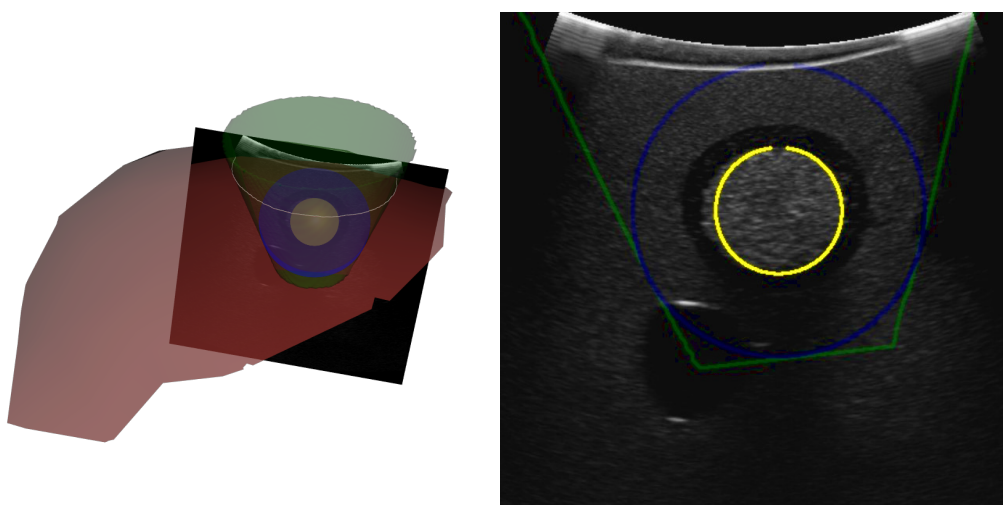


Figure 5.13. On the left side is the 3D scene with the ultrasound image cutting through the tumor, safety margin and the resection plane. On the right side is the resulting cutting overlay on the live ultrasound image. Red: Liver surface; Yellow: Tumor; Blue: Safety margin; Green: Resection plane.

5.4.2 3D model

The complete 3D scene is visualized with the VTK framework. The 3D scene contains the following differently colored models:

- Red → Liver surface
- Yellow → Tumor sphere
- Blue → Safety margin sphere
- Green → Resection plane
- White → Line indicating the resection on the liver surface

Each model (except the liver surface) in the scene can be faded in or out separately by toggling the visibilities on the control touch-screen. The liver surface, resection plane and the safety margin sphere are translucent such that surgeons can see the surgical site inside the liver intraoperatively.

5.5 UI Concept

The user interface of the software should give the surgeon confidence and accompany him safely through the operation. The software guides the surgeon step by step through the operation by telling him what he has to do next in order to continue the surgery. This informations are given to him on the 2D touch screen by different slides. The individual slides have an uniform structure (Figure 5.14). The content is in the middle, on the right side is the forward button and on the left side is the backward button. On the top is the indicator row which shows the visibility indicators for the tracked tools by the tracking camera. In the top right corner are the buttons to close the application or to take screenshots and a button to reset the view on the 3D screen.

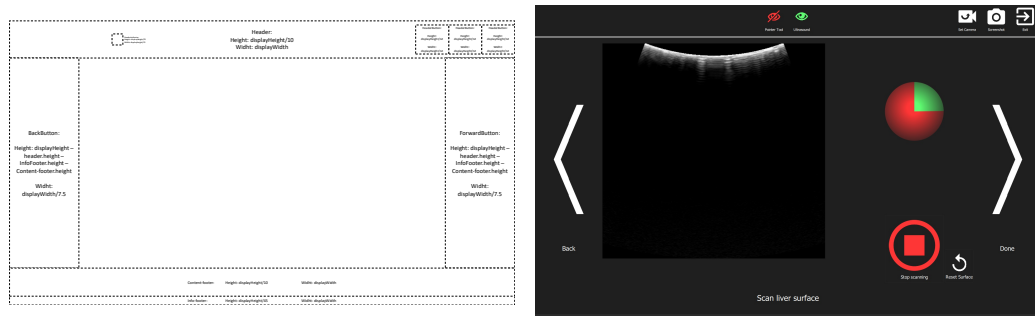


Figure 5.14. Left: The structure of the implemented user interface slides. Right: As example the seen slide while sampling the liver surface.

The content changes on each slide and the forward and backward buttons remain but change their visibility depending on the progress status on the current slide 5.14. This means the forward button is grayed out while not all requirements to continue the surgery as expected by the software are met. The backward button is not visible when it is not possible to go back to a previous slide. The content is filled with buttons and informations needed to complete the task corresponding to the current slide.



Figure 5.15. Example of a slide sequence from left to right: First, the slide before showing the ultrasound tool to the tracking camera, then the slide after showing the ultrasound and finally the slide to start the sampling of the surface.

Chapter 6

Experiments

In this chapter two experiments will be presented. The first experiment is about the accuracy of the reconstructed surface and the second experiment is about the usability of the software for surgeons.

6.1 Surface reconstruction accuracy on a technical phantom

The work presented in this section was presented at CURAC: Luca Sahli, Stefan Weber, Iwan Paolucci, "Liver surface reconstruction from navigated ultrasound during image-guided liver surgery"

It is important to know if one can rely on the reconstructed model during surgery. Therefore this experiment was done to investigate the accuracy of the reconstructed surface at different locations.

6.1.1 Methodology

To measure the accuracy of a surface it is necessary to know the true shape of the surface as accurate as possible. Because we do not know the true shape of the used liver phantom (it is always deformed a bit differently), we acquired a reference point grid which represents the true shape of the phantom. In order to do that, a regular grid with a 10 mm spacing was put on the liver phantom and with an optically tracked pointer tool each crossing point of the grid was acquired 10 times (Figure 6.1). The mean of the 10 acquisitions of one reference location lead to one 3D reference point. In this way, 414 3D reference points were created.

Afterwards 10 surface samples with the optically tracked ultrasound were acquired. The tracking cameras and the liver phantom were not moved between the acquisition of the reference points and the acquisitions of the ultrasound based samples. The 10 surfaces were reconstructed using the acquired samples. For each reference point the shortest distance to each of the reconstructed surfaces was calculated.



Figure 6.1. The regular grid (10 mm) for the reference point locations on the liver phantom used for this experiment.

6.1.2 Results

The resulting distances from the reference points to the reconstructed surfaces were statistically analyzed. The overall median distance for all the measurements is 2,57 mm with an interquartile range of 1.32 mm – 5.19 mm (Figure 6.2). Some large outliers with errors from 10 mm to 50 mm are also present. By projecting these errors corresponding to each reference point onto the liver surface, one can see that the highest errors are in segments 2 and 3 and on the right superior area of segment 7 and 8. The lowest errors are in segments 4, 5, 6 and the anterior part of segment 8 (Figure 6.3).

Distances from reference points to surfaces (mm)

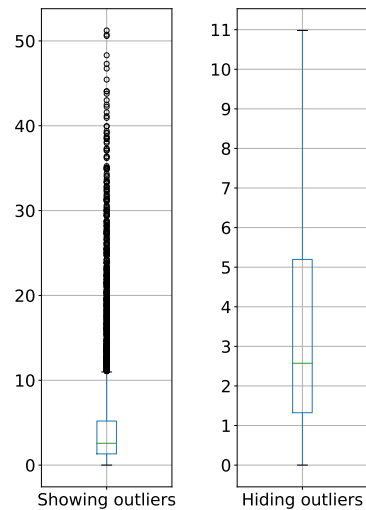


Figure 6.2. Boxplot of the distances from the reference points to the surfaces to present overall accuracy.

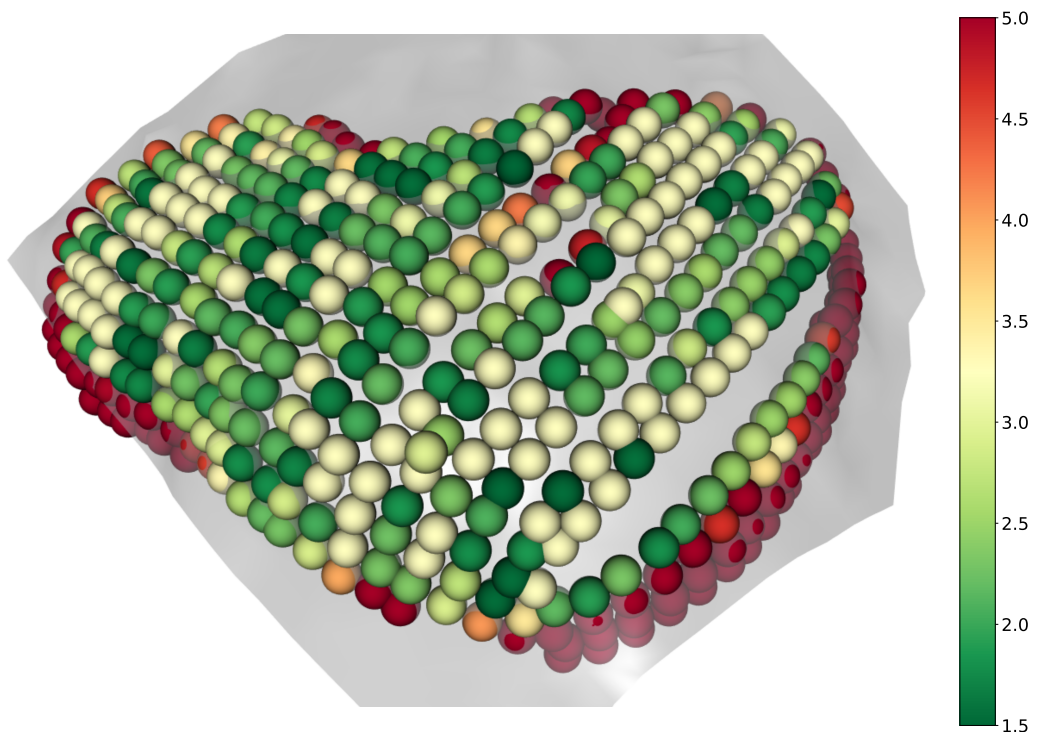


Figure 6.3. The mean distance (in mm) of each reference point visualized by colors. All points with a mean distance of over 5 mm to the surface are colored dark red. Points with a mean distance below 1.5 mm are colored dark green.

6.1.3 Discussion

Most of the anterior reference points have mean distances between 2 mm and 3 mm. These parts of the liver phantom were easier to reach with the ultrasound and also the trackable marker had a preferable orientation to the tracking camera which improves the tracking accuracy.

From a quantitative point of view, it turned out that the largest average errors are at the boundary of the liver. This is likely because these parts were probably not included in every surface scan or because the ultrasound marker was at the boundary of the tracking workspace where the tracking error is larger. But also the reconstruction of the surfaces at the boundary of the scanned area tends to be in the same plane as the principal components of the surface which also induces errors.

To conclude this experiment, the surface is better reconstructed on the anterior part of the liver than on the superior part. The boarder is poorly reconstructed and should not be trusted. However, the accuracy is good for such an early state of the project and it can hopefully be improved in the future.

6.2 Usability Test

If a new system is to be developed, an important question to ask is if the system will be used or not. The system usability scale is a reliable, often used tool for measuring the usability of a system. To find out if surgeons will use a system as presented in the previous chapters, a usability test was done with three surgeons.

6.2.1 Methodology

The surgeons tested the workflow of the developed concept on the liver phantom. After some short explanation, the surgeons had to follow the on-screen instructions of the developed software. If something was not clear to them they could ask and the unclear part was explained in more detail. Afterwards they got a questionnaire with the following 10 statements:

1. I think that I would like to use this system frequently.
2. I found the system unnecessarily complex.
3. I thought the system was easy to use.
4. I think that I would need the support of a technical person to be able to use this system.
5. I found the various functions in this system were well integrated.
6. I thought there was too much inconsistency in this system.
7. I would imagine that most people would learn to use this system very quickly.
8. I found the system very cumbersome to use.
9. I felt very confident using the system.
10. I think that I would like to use this system frequently

These statements were either answered *Strongly disagree*, *Disagree*, *Agree* or *Strongly agree*. Each answer is rated from 0 to 4 points where more points mean better usability. The points for all answers are summed up and multiplied by 2.5 to get the usability score.

6.2.2 Results

Following the on-screen instructions did work for most parts of the workflow. They all needed additional explanations for the surface scanning part. The resulting mean usability score is 79.

6.2.3 Discussion

The industry average system usability scale is 68. A score below 51 is considered insufficient and one higher as 80.3 represents a loved system that will be recommended to others. The presented system's score represents an almost loved system. A better explanation or/and feedback for the surface scanning part will be needed to improve the usability.

Additionally there are still incomplete parts in the workflow. For example only one of the selectable resection shapes actually leads to a 3D model. The others need to be implemented and it should also be possible to adjust the parameters of the resection intraoperatively which is not the case yet. With these additions the system will become more usable and loved by the surgeons.

Chapter 7

Discussion and Conclusions

In this project we developed, implemented and tested a new workflow to overcome the registration part in navigated liver surgeries. By moving an optically tracked ultrasound probe over the patients liver surface, the surface gets sampled and afterwards reconstructed using an existing reconstruction algorithm. The accuracy of the reconstructed surface was investigated in an experiment with a liver phantom and it showed that the accuracy is comparable to registration based methods [46]. Tumors can be localized with the intraoperative ultrasound and are semi-automatically segmented on a freezed image. They are approximated by a sphere and added to the 3D scene with the surface to create a more complete model of the liver. The accuracy of the tumor reconstruction is not yet analysed. The created model is used to plan the resection of the tumor. The planned resection volume is also added to the 3D scene and can be used to navigate during the surgery. A method was developed which allows to perform navigated liver operations without registration and the associated deformation problems. The expensive preoperative model and the required semi-automatic segmentations are not needed for this new approach.

The workflow compared with other navigation methods in liver surgeries changed, so a usability test was performed. Its results show that surgeons could envisage removing tumors with such a system and it is worth to investigate more time in this kind of projects.

In summary, it can be said that an accurate, intraoperative surface reconstruction on anterior part of the liver was achieved. The boundary of the reconstructed area is error-prone and should not be trusted. The method is not applicable on the posterior and inferior part of the liver because it is not reachable with the intraoperative ultrasound. The presented system is still in a prototypical state and further development is required.

Chapter 8

Outlook

So far the software was only tested on a liver phantom. Further investigations should be done to prove the applicability of the method in real patients. Therefore the software should be tested on an ex-vivo liver. Such a test could involve the removal of an artificially placed tumor and an accuracy measurement of the surface. However, also an evaluation with real patient data from a navigated liver resection could help to further analyze the correct functioning of the liver surface detector and the tumor segmentations on the ultrasound images. Additionally the liver surface detector should be extended to be able to distinguish different organs such that it does not recognize other organ's surfaces as liver surfaces.

In order to be able to navigate laproscopic resections with this method as well, the possibility to track electromagnetically should be integrated. This would lead to the method being tested and used more frequently as most resections are performed laproscopically.

Future work to continue and extend the developed concept should go in the direction of completing the 3D intraoperative reconstruction. The liver's vessel structures should be added to the model. Probably as a first step only the vessels near or in the volume affected by the planned resection.

In the current version of the software, tumors are approximated by spheres. This should be improved by adding a method to accurately reconstruct tumors automatically after semi automatic initialization. This would lead to more accurate respectation of safety margins around them. As a first step the semi automatic segmentation method should be optimized such that it works without manual corrections after the first manual initialization.

At the moment only one resection shape can be selected and it cannot be adapted. A method to adjust the resection's shape, surface entering location and safety margin would help the surgeons to create better plannings and should be added to surface. If adjusting one shape is not enough for the surgeons needs, then more shapes should added.

Bibliography

- [1] BiClamp ®: Bipolar Electrosurgical Coagulation-Effective Large-scale Coagulation of Tissue Structures in Open Surgery and Laparoscopy. Technical report.
- [2] Polaris Spectra and Vicra.
- [3] Surface Reconstruction Part II. Technical report.
- [4] D. Adalsteinsson and J. A. Sethian. A fast level set method for propagating interfaces. *Journal of Computational Physics*, 118(2):269–277, May 1995.
- [5] D. L. Aghayan, E. Pelanis, Å. A. Fretland, A. M. Kazaryan, M. A. Sahakyan, B. I. Røsok, L. Barkhatov, B. A. Bjørnbeth, O. J. Elle, and B. Edwin. Laparoscopic parenchyma-sparing liver resection for colorectal metastases. *Radiology and oncology*, 52(1):36–41, 2018.
- [6] R. Akhtar, S. Eichhorn, and P. Mummary. Microstructure-based finite element modelling and characterisation of bovine trabecular bone. *Journal of Bionic Engineering*, 3(1):3–9, Mar. 2006.
- [7] F. A. Alvarez, R. S. Claria, S. Oggero, and E. de Santibañes. Parenchymal-sparing liver surgery in patients with colorectal carcinoma liver metastases. *World journal of gastrointestinal surgery*, 8(6):407, 2016.
- [8] E. Aulisa, S. Manservisi, R. Scardovelli, and S. Zaleski. Interface reconstruction with least-squares fit and split advection in three-dimensional cartesian geometry. *Journal of Computational Physics*, 225(2):2301–2319, Aug. 2007.
- [9] U. Bagci. MEDICAL IMAGE COMPUTING (CAP 5937) LECTURE 10: Medical Image Segmentation as an Energy Minimization Problem. Technical report, Center for Research in Computer Vision (CRCV), Florida, 2016.
- [10] V. M. Banz, P. C. Müller, P. Tinguely, D. Inderbitzin, D. Ribes, M. Peterhans, D. Can-dinas, and S. Weber. Intraoperative image-guided navigation system: development and applicability in 65 patients undergoing liver surgery. *Langenbeck's archives of surgery*, 401(4):495–502, 2016.
- [11] G. Baroud. High-viscosity cement significantly enhances uniformity of cement filling in vertebroplasty: An experimental model and study on cement leakage., 2006.
- [12] S. Beller, M. Hünerbein, T. Lange, S. Eulenstei, B. Gebauer, and P. Schlag. Image-guided surgery of liver metastases by three-dimensional ultrasound-based optoelectronic navigation. *British Journal of Surgery: Incorporating European Journal of Surgery and Swiss Surgery*, 94(7):866–875, 2007.

- [13] M. Berger, A. Tagliasacchi, L. M. Seversky, P. Alliez, G. Guennebaud, J. A. Levine, A. Sharf, and C. T. Silva. A survey of surface reconstruction from point clouds. In *Computer Graphics Forum*, volume 36, pages 301–329. Wiley Online Library, 2017.
- [14] P. J. Besl and N. D. McKay. Method for registration of 3-d shapes. In *Sensor Fusion IV: Control Paradigms and Data Structures*, volume 1611, pages 586–607. International Society for Optics and Photonics, 1992.
- [15] F. Bray, J. Ferlay, I. Soerjomataram, R. L. Siegel, L. A. Torre, and A. Jemal. Global cancer statistics 2018: Globocan estimates of incidence and mortality worldwide for 36 cancers in 185 countries. *CA: a cancer journal for clinicians*, 2018.
- [16] D. M. Cash, M. I. Miga, S. C. Glasgow, B. M. Dawant, L. W. Clements, Z. Cao, R. L. Galloway, and W. C. Chapman. Concepts and preliminary data toward the realization of image-guided liver surgery. *Journal of Gastrointestinal Surgery*, 11(7):844–859, 2007.
- [17] D. M. Cash, M. I. Miga, T. K. Sinha, R. L. Galloway, and W. C. Chapman. Compensating for intraoperative soft-tissue deformations using incomplete surface data and finite elements. *IEEE transactions on medical imaging*, 24(11):1479–1491, 2005.
- [18] D. M. Cash, T. K. Sinha, W. C. Chapman, H. Terawaki, B. M. Dawant, R. L. Galloway, and M. I. Miga. Incorporation of a laser range scanner into image-guided liver surgery: surface acquisition, registration, and tracking. *Medical Physics*, 30(7):1671–1682, 2003.
- [19] D. Cherqui, E. Husson, R. Hammoud, B. Malassagne, F. Stéphan, S. Bensaid, N. Rotman, and P.-L. Fagniez. Laparoscopic liver resections: a feasibility study in 30 patients. *Annals of surgery*, 232(6):753, 2000.
- [20] L.-C. Chu and C.-C. Chang. Infrared 3d scanning system, Aug. 27 2002. US Patent 6,442,419.
- [21] L. W. Clements, J. A. Collins, J. A. Weis, A. L. Simpson, T. P. Kingham, W. R. Jarnagin, and M. I. Miga. Deformation correction for image guided liver surgery: An intraoperative fidelity assessment. *Surgery*, 162(3):537–547, 2017.
- [22] L. W. Clements, J. A. Collins, Y. Wu, A. L. Simpson, W. R. Jarnagin, and M. I. Miga. Validation of model-based deformation correction in image-guided liver surgery via tracked intraoperative ultrasound: preliminary method and results. In *Medical Imaging 2015: Image-Guided Procedures, Robotic Interventions, and Modeling*, volume 9415, page 94150T. International Society for Optics and Photonics, 2015.
- [23] W. Commons. Local outlier factor, 2018. LOF.svg.
- [24] Y. Cui and D. Stricker. 3d shape scanning with a kinect. In *ACM SIGGRAPH 2011 Posters*, page 57. ACM, 2011.
- [25] B. Dagon, C. Baur, and V. Bettschart. Real-time update of 3d deformable models for computer aided liver surgery. In *Pattern Recognition, 2008. ICPR 2008. 19th International Conference on*, pages 1–4. IEEE, 2008.
- [26] M. Dou, J. Taylor, H. Fuchs, A. Fitzgibbon, and S. Izadi. 3d scanning deformable objects with a single rgbd sensor. In *Proceedings of the IEEE Conference on Computer Vision and Pattern Recognition*, pages 493–501, 2015.

- [27] A. Ferrero, R. L. Tesoriere, S. Langella, and N. Russolillo. Parenchymal-Sparing Liver Resections, pages 249–264. Springer International Publishing, Cham, 2017.
- [28] J. G. D. Franca, M. A. Gazziro, A. N. Ide, and J. H. Saito. A 3d scanning system based on laser triangulation and variable field of view. In Image Processing, 2005. ICIP 2005. IEEE International Conference on, volume 1, pages I–425. IEEE, 2005.
- [29] Y. Furukawa and J. Ponce. Accurate, dense, and robust multiview stereopsis. IEEE transactions on pattern analysis and machine intelligence, 32(8):1362–1376, 2010.
- [30] D. Galun, D. Basaric, M. Zuvela, P. Bulajic, A. Bogdanovic, N. Bidzic, and M. Milicevic. Hepatocellular carcinoma: From clinical practice to evidence-based treatment protocols. World journal of hepatology, 7(20):2274, 2015.
- [31] O. Heizmann, S. Zidowitz, H. Bourquin, S. Potthast, H.-O. Peitgen, D. Oertli, and C. Kettelhack. Assessment of intraoperative liver deformation during hepatic resection: prospective clinical study. World journal of surgery, 34(8):1887–1893, 2010.
- [32] H. Hoppe, T. DeRose, T. Duchamp, J. McDonald, and W. Stuetzle. Surface reconstruction from unorganized points, volume 26. ACM, 1992.
- [33] A. Hornung and L. Kobbelt. Robust reconstruction of watertight 3 d models from non-uniformly sampled point clouds without normal information. In Symposium on geometry processing, pages 41–50. Citeseer, 2006.
- [34] M. Kazhdan. Reconstruction of solid models from oriented point sets. In Proceedings of the third Eurographics symposium on Geometry processing, page 73. Eurographics Association, 2005.
- [35] T. P. Kingham, S. Jayaraman, L. W. Clements, M. A. Scherer, J. D. Stefansic, and W. R. Jarnagin. Evolution of image-guided liver surgery: transition from open to laparoscopic procedures. Journal of Gastrointestinal Surgery, 17(7):1274–1282, 2013.
- [36] T. Lange, S. Eulenstein, M. Hünerbein, and P.-M. Schlag. Vessel-based non-rigid registration of mr/ct and 3d ultrasound for navigation in liver surgery. Computer Aided Surgery, 8(5):228–240, 2003.
- [37] T. Lange, N. Papenberg, S. Heldmann, J. Modersitzki, B. Fischer, H. Lamecker, and P. M. Schlag. 3d ultrasound-ct registration of the liver using combined landmark-intensity information. International journal of computer assisted radiology and surgery, 4(1):79–88, 2009.
- [38] T. Langø, S. Vijayan, A. Rethy, C. Våpenstad, O. V. Solberg, R. Märvik, G. Johnsen, and T. N. Hernes. Navigated laparoscopic ultrasound in abdominal soft tissue surgery: technological overview and perspectives. International journal of computer assisted radiology and surgery, 7(4):585–599, 2012.
- [39] R. Lencioni and L. Crocetti. Local-regional treatment of hepatocellular carcinoma. Radiology, 262(1):43–58, 2012.
- [40] M. Levoy, K. Pulli, B. Curless, S. Rusinkiewicz, D. Koller, L. Pereira, M. Ginzton, S. Anderson, J. Davis, J. Ginsberg, et al. The digital michelangelo project: 3d scanning of large statues. In Proceedings of the 27th annual conference on Computer graphics and interactive techniques, pages 131–144. ACM Press/Addison-Wesley Publishing Co., 2000.

- [41] H. Li, Y. Li, R. Yu, J. Sun, and J. Kim. Surface reconstruction from unorganized points with l0 gradient minimization. *Computer Vision and Image Understanding*, 169:108–118, 2018.
- [42] S. P. Lim and H. Haron. Surface reconstruction techniques: a review. *Artificial Intelligence Review*, 42(1):59–78, 2014.
- [43] A. H. Mahnken, K. E. Wilhelm, J. Ricke, et al. *CT-and MR-guided Interventions in Radiology*, volume 22. Springer, 2009.
- [44] L. Maier-Hein, A. Groch, A. Bartoli, S. Bodenstedt, G. Boissonnat, P.-L. Chang, N. Clancy, D. S. Elson, S. Haase, E. Heim, et al. Comparative validation of single-shot optical techniques for laparoscopic 3-d surface reconstruction. *IEEE transactions on medical imaging*, 33(10):1913–1930, 2014.
- [45] S. McGuire. World cancer report 2014. geneva, switzerland: World health organization, international agency for research on cancer, who press, 2015, 2016.
- [46] W. H. Nam, D.-G. Kang, D. Lee, J. Y. Lee, and J. B. Ra. Automatic registration between 3d intra-operative ultrasound and pre-operative ct images of the liver based on robust edge matching. *Physics in Medicine & Biology*, 57(1):69, 2011.
- [47] D. A. North, R. T. Groeschl, D. Sindram, J. B. Martinie, D. A. Iannitti, M. Bloomston, C. Schmidt, W. S. Rilling, T. C. Gamblin, and R. C. Martin. Microwave ablation for hepatic malignancies: a call for standard reporting and outcomes. *The American Journal of Surgery*, 208(2):284–294, 2014.
- [48] K. Numminen, O. Sipilä, and H. Mäkipalo. Preoperative hepatic 3d models: virtual liver resection using three-dimensional imaging technique. *European journal of radiology*, 56(2):179–184, 2005.
- [49] D. K. Pai, K. v. d. Doel, D. L. James, J. Lang, J. E. Lloyd, J. L. Richmond, and S. H. Yau. Scanning physical interaction behavior of 3d objects. In *Proceedings of the 28th annual conference on Computer graphics and interactive techniques*, pages 87–96. ACM, 2001.
- [50] Y. Payan. *Soft tissue biomechanical modeling for computer assisted surgery*, volume 11. Springer, 2012.
- [51] M. Peterhans, S. Anderegg, P. Gaillard, T. Oliveira-Santos, and S. Weber. A fully automatic calibration framework for navigated ultrasound imaging. In *Engineering in Medicine and Biology Society (EMBC), 2010 Annual International Conference of the IEEE*, pages 1242–1245. IEEE, 2010.
- [52] M. Peterhans, A. vom Berg, B. Dagon, D. Inderbitzin, C. Baur, D. Candinas, and S. Weber. A navigation system for open liver surgery: design, workflow and first clinical applications. *The International Journal of Medical Robotics and Computer Assisted Surgery*, 7(1):7–16, 2011.
- [53] F. Pianka, M. Baumhauer, D. Stein, B. Radeleff, B. M. Schmied, H.-P. Meinzer, and S. A. Müller. Liver tissue sparing resection using a novel planning tool. *Langenbeck's archives of surgery*, 396(2):201–208, 2011.
- [54] G. Postelnicu, L. Zollei, and B. Fischl. Combined volumetric and surface registration. *IEEE transactions on medical imaging*, 28(4):508–522, 2009.

- [55] T. Ramos. A review of surface matching models: perspectives and challenges for automatic soft-tissue registration in computer-assisted interventions. *Revista E-Tech: Tecnologias para Competitividade Industrial-ISSN-1983-1838*, 8(2):143–184, 2015.
- [56] D. Reichard, D. Häntschi, S. Bodenstedt, S. Suwelack, M. Wagner, H. Kenngott, B. Müller-Stich, L. Maier-Hein, R. Dillmann, and S. Speidel. Projective biomechanical depth matching for soft tissue registration in laparoscopic surgery. *International journal of computer assisted radiology and surgery*, 12(7):1101–1110, 2017.
- [57] D. Ribes, M. Peterhans, S. Anderegg, D. Wallach, V. Banz, C. Kim-Fuchs, D. Candinas, and S. Weber. Image guided liver surgery. *Int J CARS*, 7(1):S141–S145, 2012.
- [58] D. Ribes¹, M. Peterhans, D. Wallach, V. Banz, G. Stavrou, and S. Weber. Surface based us/mevis-ct registration for open liver surgery.
- [59] D. C. Rucker, Y. Wu, L. W. Clements, J. E. Ondrasek, T. S. Pheiffer, A. L. Simpson, W. R. Jarnagin, and M. I. Miga. A mechanics-based nonrigid registration method for liver surgery using sparse intraoperative data. *IEEE transactions on medical imaging*, 33(1):147–158, 2014.
- [60] J. Salvi, J. Pages, and J. Batlle. Pattern codification strategies in structured light systems. *Pattern recognition*, 37(4):827–849, 2004.
- [61] A. L. Simpson and T. P. Kingham. Current evidence in image-guided liver surgery. *Journal of Gastrointestinal Surgery*, 20(6):1265–1269, 2016.
- [62] A. K. Siriwardena, J. M. Mason, S. Mullamitha, H. C. Hancock, and S. Jegatheeswaran. Management of colorectal cancer presenting with synchronous liver metastases. *Nature reviews Clinical oncology*, 11(8):446, 2014.
- [63] S. Speidel, S. Roehl, S. Suwelack, R. Dillmann, H. Kenngott, and B. Mueller-Stich. Intraoperative surface reconstruction and biomechanical modeling for soft tissue registration. In *Proc. Joint Workshop on New Technologies for Computer/Robot Assisted Surgery*, pages 0–0, 2011.
- [64] S. Thompson, J. Totz, Y. Song, S. Johnsen, D. Stoyanov, S. Ourselin, K. Gurusamy, C. Schneider, B. Davidson, D. Hawkes, et al. Accuracy validation of an image guided laparoscopy system for liver resection. In *Medical Imaging 2015: Image-Guided Procedures, Robotic Interventions, and Modeling*, volume 9415, page 941509. International Society for Optics and Photonics, 2015.
- [65] G. Torzilli. *Ultrasound guided liver surgery*. Springer, 2014.
- [66] Wikipedia contributors. Maximum flow problem — Wikipedia, the free encyclopedia, 2018. [Online; accessed 15-October-2018].
- [67] A. D. Wiles, D. G. Thompson, and D. D. Frantz. Accuracy assessment and interpretation for optical tracking systems. In *Medical Imaging 2004: Visualization, Image-Guided Procedures, and Display*, volume 5367, pages 421–433. International Society for Optics and Photonics, 2004.
- [68] R. Wu, K. V. Ling, W. Shao, and W. S. Ng. Registration of organ surface with intraoperative 3d ultrasound image using genetic algorithm. In *International Conference on Medical Image Computing and Computer-Assisted Intervention*, pages 383–390. Springer, 2003.

- [69] Y. Yu. Surface reconstruction from unorganized points using self-organizing neural networks. In IEEE Visualization, volume 99, pages 61–64. Citeseer, 1999.
- [70] Y.-j. Zhao, D.-c. Zhou, F.-b. Liu, H.-c. Zhao, G.-b. Wang, and X.-p. Geng. Biclamp® vessel-sealing device for open hepatic resection of malignant and benign liver tumours: a single-institution experience. BMC cancer, 17(1):554, 2017.

etc.

Appendices

Appendix A

Vector and Tensor Mathematics

A.1 Introduction

...

A.2 Variable Types

...

Appendix B

Another Appendix

B.1 Section 1

...

B.2 Section 2

...